

Coupling Analysis of the Asymptotic Behaviour of a Primal-Dual Langevin Algorithm

Martin Burger^{1,2}, Matthias J. Ehrhardt³, Lorenz Kuger^{1,4,*}, and Lukas Weigand¹

¹Helmholtz Imaging, Deutsches Elektronen-Synchrotron DESY, Notkestr. 85, 22607 Hamburg, Germany.

²Fachbereich Mathematik, Universität Hamburg, Bundesstrasse 55, Hamburg, 20146, Germany.

³Department of Mathematical Sciences, University of Bath, Claverton Down, Bath BA2 7AY, United Kingdom.

⁴Department Mathematik, Friedrich-Alexander-Universität Erlangen-Nürnberg, Cauerstr. 11, 91058 Erlangen, Germany.

*Corresponding author – lorenz.kuger@desy.de

May 30, 2024

Abstract

We analyze a recently proposed algorithm for the problem of sampling from probability distributions μ^* in \mathbb{R}^d with a Lebesgue density of the form $\mu^*(x) \propto \exp(-f(Kx) - g(x))$, where K is a linear operator and f, g convex and non-smooth. The algorithm is a generalization of the primal-dual hybrid gradient (PDHG) convex optimization algorithm to a sampling scheme. We analyze the method's continuous time limit, an SDE in the joint primal-dual variable. We give mild conditions under which the corresponding Fokker-Planck equation converges to a unique stationary state, which however does not concentrate in the dual variable and consequently does not have μ^* as its primal marginal. Under a smoothness assumption on f , we show that the scheme converges to the purely primal overdamped Langevin diffusion in the limit of small primal and large dual step sizes. We further prove that the target can never be the primal marginal of the invariant solution for any modification of the SDE with space-homogeneous diffusion coefficient. A correction with inhomogeneous diffusion coefficient and the correct invariant solution is proposed, but the scheme requires the same smoothness assumptions on f and is numerically inferior to overdamped Langevin diffusion. We demonstrate our findings numerically first on small-scale examples in which we can exactly verify the theoretical results, and subsequently on typical examples of larger scale from Bayesian imaging inverse problems.

1 Introduction

We analyze a recently proposed algorithm for sampling from a probability distribution on $\mathcal{X} := \mathbb{R}^d$ with log-concave, non-smooth density. In particular, we are interested in sampling from target distributions with Lebesgue densities of the form

$$\mu^*(x) = \frac{\exp(-f(Kx) - g(x))}{\int \exp(-f(Kw) - g(w)) dw}, \quad (1.1)$$

where we assume that the integral in the denominator exists and is finite. The operator $K : \mathcal{X} \rightarrow \mathbb{R}^m$ is assumed to be linear and $f : \mathcal{Y} \rightarrow \mathbb{R} \cup \{\infty\}$, $g : \mathcal{X} \rightarrow \mathbb{R} \cup \{\infty\}$ will be called potential

terms and are both assumed convex and lower semi-continuous but not necessarily differentiable. We will denote the full potential by $f \circ K + g =: h : \mathcal{X} \rightarrow \mathbb{R} \cup \{\infty\}$.

A standard class of algorithms to draw samples in Bayesian inference are Markov chain Monte Carlo (MCMC) methods. Compared to other types of MCMC methods, sampling schemes based on Langevin diffusion processes have proved efficient in inverse problems and imaging applications due to their preferable scaling behaviour to high dimensions [7, 17, 33]. MCMC sampling algorithms based on Langevin diffusion typically perform a time discretisation of the stochastic differential equation (SDE)

$$X_t = \nabla \log \mu^*(X_t) dt + \sqrt{2} dW_t, \quad (1.2)$$

where W_t is standard \mathbb{R}^d -valued Brownian motion. Assuming μ^* satisfies a log-Sobolev inequality, it is the unique invariant distribution of the SDE and the law of X_t will converge to μ^* as t grows. The standard Euler-Maruyama discretization of (1.2) takes the form

$$\begin{cases} \xi^{n+1} \sim N(0, I_d) \\ X^{n+1} = X^n + \tau \nabla \log \mu^*(X_k) + \sqrt{2\tau} \xi^{n+1}, \end{cases} \quad (1.3)$$

this iteration is also known as unadjusted Langevin algorithm (ULA). ULA and also similar implicit or semi-implicit time discretizations introduce a bias between the law of the samples and the target measure, hence many works have been concerned with the characterization of the invariant distribution of the Markov chain (X^n) and its bias [15, 21, 23, 33]. Further questions typically concern preconditioning and convergence speed of the Markov chain and the behaviour of Metropolis-Hastings correction steps to overcome the bias and draw unbiased samples from μ^* .

In this work, we are concerned with a new type of Langevin sampling algorithm which has been proposed as *Unadjusted Langevin Primal-Dual Algorithm* (ULPDA) in [10] and has since been mentioned in [3, 5]. Unlike ULA or its variants, ULPDA can not be interpreted as a time discretization of (1.2). The algorithm consists in carrying out steps of a primal-dual optimization method, where the same type of stochasticity as in unadjusted Langevin algorithms is added to the primal variable in each step. Its motivation is hence inspired by the optimization view: Just as (1.3) can be interpreted as a gradient descent with an additive stochastic component, one might be able to obtain more general sampling algorithms by adding the right amount of stochasticity to more general classes of first-order optimization methods. This is, of course, not a rigorous argument for convergence, and until now, to the best of the authors' knowledge, no convergence theory for ULPDA has been provided. Indeed, the situation seems to be more intricate: When we run ULPDA on a simple toy example, the distribution of the samples seems to depend more critically on the choice of step size hyperparameters τ, σ of the algorithm than it is known from ULA, see Figure 1.

1.1 Related Works

There is a vast literature on unadjusted Langevin algorithms, where we use the term to refer not only to (1.3), but any time discretization of (1.2). The analysis is based on the fact that the target distribution is the stationary distribution of the SDE (1.2) and that the dynamics converge to the target in continuous time [33]. This is based on the fact that the dynamics can be understood as a gradient flow of relative entropy with respect to the target in Wasserstein space [21, 32]. Standard convergence results on ULA typically require a Lipschitz continuous gradient of the potential in order to bound the error introduced by time discretization [15, 16, 17].

Since non-smooth densities do not satisfy this gradient Lipschitz condition, many works have treated the extension to the non-smooth case. Generally, the approaches can be divided into two classes. The first regularizes non-smooth terms, resulting in a modified, smooth target and applies typical ULA to

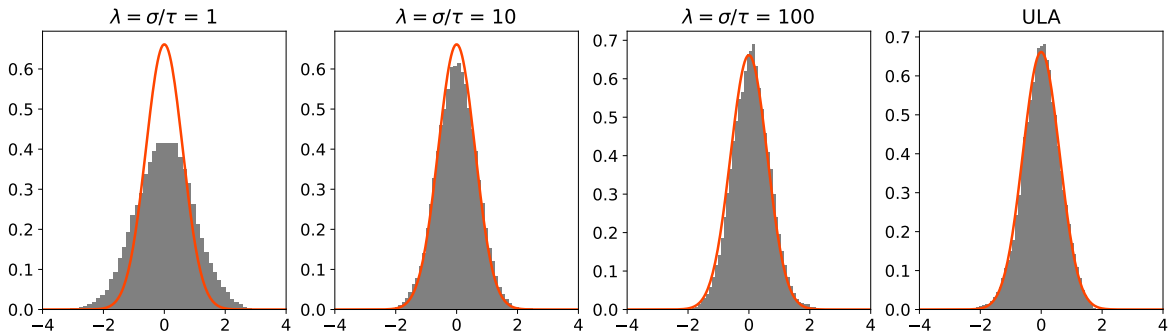


Figure 1: In a simple toy example, we choose $f, g : \mathbb{R} \rightarrow \mathbb{R}$ to be quadratic functions, $K > 0$ a real number, so that the target μ^* is Gaussian with the density depicted in orange. We run ULPDA with very small primal step size τ and sufficient burn-in period and repeat the experiment for three different ratios σ/τ . The gray histograms show the distribution of samples produced by ULPDA. For comparison, the right figure is produced by ULA with the same primal step size τ .

this modified distribution. The challenge then typically consists in bounding the terms between the target and the modified distribution, and numerically in trading off the introduced bias and convergence speed via the smoothing parameter [1, 7, 8, 20, 25]. The second approach consists in finding different discretizations of (1.2), i.e. implicit or semi-implicit schemes, that are implementable and provably convergent. These schemes are usually referred to as proximal or implicit Langevin methods, see e.g. [2, 4, 14, 18, 25]. A work of particular relevance for our setting is [3], since the authors assume the same type of splitting of the potential $h = f \circ K + g$ as we do. Their method ‘Prox-Sub’ can be understood as a first-order forward-backward discretization of (1.2), with the forward step in $f \circ K$ realized as a subgradient since f is assumed non-smooth. We will see that this method is intimately connected to the primal-dual sampling algorithm since it forms the limiting case in which the primal-dual stationary distribution can be related to the target. In [10], the authors proposed the primal-dual scheme that we consider here, in order to generalize from the class of methods that employ purely primal discretizations of (1.2). A partial dualization of the potential is also considered in [1], although their analysis still requires the relevant part f of the potential to be smooth. We also refer to [5] for a recent comparison of current methods applicable in the non-smooth case.

Constraints on the state space can be viewed as a special case of non-smooth potentials, where the constraint is enforced by adding an indicator function to the potential. Several works have considered this special case usually by incorporating a proximal (which amounts to a projection in the case of an indicator) or a reflection step [6, 19, 22]. Mirroring the Langevin dynamics can be another approach to precondition the dynamics as well as to enforce geometrical constraints [8, 9, 11, 30].

1.2 Contributions

- For the continuous time limit of the iteration, we prove a contraction result using a coupling argument, which makes the dynamics asymptotically stable and guarantees convergence to the corresponding stationary solution.
- We show that the marginal with respect to the primal variable of the stationary solution in continuous time is not the target distribution. This can be interpreted as being a consequence of the dynamics not concentrating in the dual variable, although the diffusion coefficient is degenerate with the stochastic term only added to the primal variable.
- We consider two potential frameworks for “correcting” the bias between continuous time station-

ary and target distribution. A proposed modification of the dynamics with non-homogeneous diffusion coefficient can be employed to force the target to become the stationary solution. Secondly, we consider the unmodified scheme, but with the ratio of primal and dual step sizes in the algorithm growing to infinity. In the limit, the stationary distribution of the unmodified scheme is shown to converge to the target under regularity assumptions on the dualized potential.

- In discrete time, we show stability of the algorithm in the sense that Wasserstein distances between two different instances are bounded if the potentials are convex. Under stronger regularity assumptions on f^*, g , there exists a stationary solution to which the distribution of the iterates converges.

The manuscript is organized as follows. In Section 2, we give the considered sampling procedure based on primal-dual optimization and derive its continuous time limit SDE. Since this limiting SDE differs from (1.2), we devote Section 3 to the analysis of the continuous time setting. We derive the mean-field limit Fokker-Planck equation and show contraction properties in Section 3.1. In Section 3.2, we prove a central ‘negative’ result, i.e. that the target can not be the stationary distribution for any homogeneous diffusion coefficient and illustrate the (non-)concentration of the mean-field limit, which is crucial to understand how its stationary state relates to the target distribution. This relation is proven in Section 3.3, which allows to bound the bias due to the dualization in Wasserstein distance. We further show that the PDE can be modified to force the target to be its stationary distribution by employing a non-homogeneous diffusion coefficient. By transferring some of the time continuous arguments to the discretized algorithm and using typical computations known from primal-dual optimization methods, we show stability of the algorithm and convergence to a stationary state in Section 4. We present numerical illustrations of our most important findings in Section 5

2 The Primal-Dual Sampling Scheme

Although the algorithmic approach is not limited to this setting, in the context of Bayesian inference, the target distribution μ^* is typically a posterior distribution. Such a posterior target is defined through the likelihood $p(z|x)$ of observing z given the true parameter x , combined with a prior distribution $p(x)$. It is given by

$$p(x|z) = \frac{1}{Z} p(z|x)p(x),$$

where the normalization constant $Z = \int p(z|w)p(w) dw$ is typically intractable in high dimensions. As an example class of problems that we consider, in Bayesian inference for imaging inverse problems the distributions are typically high-dimensional and involve non-smooth terms. This is because model-based priors on image distributions often assume sparse coefficients in some basis, the recovery of which corresponds to minimization of non-smooth functions [31]. Therefore, many relevant posteriors $p(x|z)$ fall into the class of targets given in (1.1). We start by explaining the motivation for the primal-dual sampling from the point of view of convex, non-smooth optimization.

2.1 Motivation for ULPDA

A common task in Bayesian inverse problems is the computation of the maximum a posteriori estimate (MAP), i.e. the mode of the distribution $\mu^* = p(\cdot|z)$. This task forms the connection between Bayesian formulations of inverse problems and variational regularization approaches, since it amounts to the problem of computing the solution to the following minimization problem

$$\arg \min_x f(Kx) + g(x). \tag{2.1}$$

In order to solve (2.1), depending on the structure of f , K and g it can be helpful to employ techniques from convex duality on parts of the potential $h = f \circ K + g$. A popular approach consists in reformulating the variational problem (2.1) to the saddle point problem

$$\begin{aligned} \min_x h(x) &= \min_x (g(x) + \max_y (\langle Kx, y \rangle - f^*(y))) \\ &= \min_x \max_y s(x, y) \end{aligned} \quad (2.2)$$

with $s(x, y) := g(x) + \langle Kx, y \rangle - f^*(y)$. Here f^* denotes the convex conjugate of f defined by

$$f^*(y) := \sup_x \{ \langle x, y \rangle - f(x) \}.$$

Under mild assumptions on g and f^* , one can prove existence of a saddle point (x^*, y^*) (see section 19 in [28] for details) the primal part x^* of which is a solution to the original problem (2.1). Instead of minimizing h , one can then employ primal-dual type algorithms to solve the saddle point problem (2.2). For the context of imaging inverse problems, we refer to [24] for an overview.

The primal-dual optimization method (primal descent and dual ascent with extrapolation) for (2.2) takes the form

$$\begin{cases} Y^{n+1} = \text{prox}_{\sigma f^*}(Y^n + \sigma K X_\theta^n) \\ X^{n+1} = \text{prox}_{\tau g}(X^n - \tau K^T Y^n) \\ X_\theta^{n+1} = X^{n+1} + \theta(X^{n+1} - X^n) \end{cases} \quad (2.3)$$

with step sizes τ and σ and a relaxation parameter θ chosen accordingly. Herein, the proximal operator for a convex functional φ and a step size $\gamma > 0$ is defined by

$$\text{prox}_{\gamma\varphi}(z) := (id + \gamma\partial\varphi)^{-1}(z) = \arg \min_w \left\{ \varphi(w) + \frac{1}{2\gamma} \|w - z\|_2^2 \right\}.$$

The minimum is attained by a unique point, and the application of the proximal operator can be viewed as an implicit time step in the gradient flow of the functional φ . For convergence theory of the scheme (2.3) and possible accelerations we refer to [24, 29].

In order to draw the parallels between computing the MAP of μ^* and drawing samples from μ^* , we want to recall the standard unadjusted Langevin algorithm (1.3). Under appropriate conditions on h and the step size τ , ULA converges to a stationary distribution whose distance to the target μ^* can be bounded by a factor depending on h and the considered metric on the space of probability distributions [15]. ULA can be interpreted as a scheme alternating a gradient descent step in h and a diffusion step (or, equivalently, a time step along the gradient flow of entropy in the Wasserstein space). In particular, the additional diffusion step ensures the samples have the correct covariance (up to a bias scaling linearly in the step size τ).

It appears natural to take a similar perspective for primal-dual optimization methods and add a diffusion step at some point in the iteration. Such a scheme was proposed (without further theoretical analysis) under the name unadjusted Langevin primal-dual algorithm (ULPDA) in [10]. The iteration takes the form

$$\begin{cases} Y^{n+1} = \text{prox}_{\sigma f^*}(Y^n + \sigma K X_\theta^n) \\ \xi^{n+1} \sim \text{N}(0, I_d) \\ X^{n+1} = \text{prox}_{\tau g}(X^n - \tau K^T Y^n) + \sqrt{2\tau} \xi^{n+1} \\ X_\theta^{n+1} = X^{n+1} + \theta(X^{n+1} - X^n), \end{cases} \quad (2.4)$$

where the diffusion step is added in the primal variable X_k and the overrelaxation parameter θ was set to $\theta = 1$ in [10] in the spirit of primal-dual optimization methods. Note that the stochastic term in the update for X^{n+1} may be added in the argument of the proximal operator (as in [10]) or after applying the proximal operator (as in 2.4). For the considerations in continuous time, this makes no difference, however it will simplify some of our analysis in discrete time based on couplings in Section 4.

2.2 Continuous time perspective

In the analysis of ULA's convergence behaviour, it is helpful to view the update step as an Euler-Maruyama time discretization of the overdamped Langevin diffusion (1.2). Convergence results for ULA are based on the fact that the target measure μ^* is the unique invariant distribution of the Markov process X_t .

In order to analyze ULPDA, we want to define a similar time-continuous limit of (2.4). For that, we assume that the step sizes τ, σ are coupled via a parameter $\lim_{\tau, \sigma \rightarrow 0} \frac{\sigma}{\tau} = \lambda$. Taking both step sizes to zero at this ratio, the formal limiting Markov process satisfies the diffusion equation

$$\begin{cases} dX_t \in -(\partial g(X_t) + K^* Y_t) dt + \sqrt{2} dW_t \\ dY_t \in -\lambda(\partial f^*(Y_t) - K X_t) dt, \end{cases} \quad (2.5)$$

which we can write in a joint variable $Z_t = (X_t, Y_t)$ as

$$dZ_t \in -A_{\text{cPD}}(Z_t) dt + B_{\text{cPD}} dW_t. \quad (2.6)$$

where we introduced the continuous-time primal-dual coefficients

$$A_{\text{cPD}}(Z_t) = \begin{pmatrix} \partial g & K^T \\ -\lambda K & \lambda \partial f^* \end{pmatrix}, \quad B_{\text{cPD}} = \begin{pmatrix} \sqrt{2} I \\ 0 \end{pmatrix}, \quad (2.7)$$

with I the identity in \mathbb{R}^d . Note in particular that the diffusion coefficient $\Sigma_{\text{cPD}} = \frac{1}{2} B_{\text{cPD}} B_{\text{cPD}}^T$ is only positive semi-definite (or degenerate) with an m -dimensional null space, where m is the dimension of the dual variable Y . As we will see in more detail, the corresponding mean-field limit PDE is not elliptic anymore, which complicates analysis of existence and uniqueness of solutions.

2.3 Spaces and notation

We denote by $\mathcal{P}(\mathbb{R}^d)$ the space of probability measures on \mathbb{R}^d , and by $\mathcal{P}_p(\mathbb{R}^d)$ the subspace of distributions with finite p -th moment. Given a norm $\|\cdot\|$ on \mathbb{R}^d , a transport distance on $\mathcal{P}_2(\mathbb{R}^d)$ can be defined by

$$\mathcal{T}(\mu, \tilde{\mu}) := \inf_{\mathcal{M} \in \Gamma(\mu, \tilde{\mu})} \left(\mathbb{E}_{(x, \tilde{x}) \sim \mathcal{M}} [\|x - \tilde{x}\|^2] \right)^{1/2}.$$

where $\Gamma(\mu, \tilde{\mu})$ denotes the set of all couplings with marginals μ and $\tilde{\mu}$

$$\Gamma(\mu, \tilde{\mu}) = \left\{ \mathcal{M} \in \mathcal{P}(\mathbb{R}^n \times \mathbb{R}^n) : \mu = \int_{\mathbb{R}^n} \mathcal{M}(\cdot, \tilde{x}) d\tilde{x} \text{ and } \tilde{\mu} = \int_{\mathcal{X}} \mathcal{M}(x, \cdot) dx \right\}.$$

\mathcal{T} defines a metric on $\mathcal{P}_2(\mathbb{R}^d)$. If $\|\cdot\|$ is the Euclidean norm, then \mathcal{T} is the 2-Wasserstein distance \mathcal{W}_2 .

In the following, we will denote the state spaces $\mathcal{X} = \mathbb{R}^d$ for the primal and $\mathcal{Y} = \mathbb{R}^m$ for the dual variable. In order to simplify notation, we introduce a weighted inner product and norm on the product space $\mathcal{Z} := \mathcal{X} \times \mathcal{Y}$. For a scalar $a > 0$, we define $\langle \cdot, \cdot \rangle_a$ on \mathcal{X} (and analogously on \mathcal{Y}) by $\langle x, \tilde{x} \rangle_a := \langle ax, \tilde{x} \rangle$ for all $x, \tilde{x} \in \mathcal{X}$, where $\langle \cdot, \cdot \rangle$ is the Euclidean inner product on \mathcal{X} . Further, denote by $\|\cdot\|_a$ the weighted norm $\|x\|_a = \sqrt{\langle x, x \rangle_a}$. Given $a, b > 0$, we define a weighted inner product on the product space \mathcal{Z} by

$$\langle z, \tilde{z} \rangle_{a,b} = \langle x, \tilde{x} \rangle_a + \langle y, \tilde{y} \rangle_b, \quad z = (x, y), \tilde{z} = (\tilde{x}, \tilde{y}) \in \mathcal{Z}.$$

Accordingly, we define a weighted norm by

$$\|z\|_{a,b} := \sqrt{\langle z, z \rangle_{a,b}} = \sqrt{\|x\|_a^2 + \|y\|_b^2}, \quad z = (x, y) \in \mathcal{Z}.$$

On the space $\mathcal{P}(\mathcal{Z})$, we will also denote $\mathcal{T}_{a,b}$ for the transport distance induced by the norm $\|\cdot\|_{a,b}$. Note that $\mathcal{T}_{a,b}$ is a metric on $\mathcal{P}_2(\mathcal{Z})$ and $\mathcal{T}_{1,1} = \mathcal{W}_2$. For every $a, b > 0$, $\mathcal{T}_{a,b}$ is equivalent to \mathcal{W}_2 , since the fact $\sqrt{\min\{a,b\}} d_{1,1}(z, \tilde{z}) \leq d_{a,b}(z, \tilde{z}) \leq \sqrt{\max\{a,b\}} d_{1,1}(z, \tilde{z})$ directly implies

$$\sqrt{\min\{a,b\}} \mathcal{W}_2 \leq \mathcal{T}_{a,b} \leq \sqrt{\max\{a,b\}} \mathcal{W}_2.$$

3 The Stationary Solution in Continuous Time

We start by proving the existence of a unique stationary solution of the time-continuous limit (2.6) of the ULPDA algorithm. We further show that the corresponding primal-dual Fokker-Planck equation is contractive, implying convergence of any solution path to the stationary distribution. The contraction result is formulated for a general class of diffusion SDEs. It follows a standard calculation from the literature for overdamped Langevin diffusion and is generalized to the setting of an SDE with any strongly monotone operator as non-homogeneous drift coefficient.

3.1 Fokker-Planck Equation and Existence of a Stationary Solution

3.1.1 Contraction of Overdamped Langevin Diffusion via Coupling Argument

Suppose for now that the potential $h : \mathcal{X} \rightarrow \mathbb{R}$ is differentiable, that ∇h is L -Lipschitz-continuous and ω_h -strongly convex. We repeat here an instructive calculation that has been carried out, e.g., in [13, 17] to show stability of the overdamped Langevin diffusion process

$$dX_t = -\nabla h(X_t)dt + \sqrt{2}dW_t. \quad (3.1)$$

The distribution μ_t of the process X_t in (3.1), denoted $\mu_t = \text{Law}(X_t)$, satisfies the Fokker-Planck equation (or forward Kolmogorov equation) [27] given by

$$\frac{\partial \mu_t}{\partial t} = \nabla_x \cdot (\mu_t \nabla h(x)) + \Delta_x \mu_t.$$

The target distribution μ^* is the unique stationary solution of the Fokker-Planck equation. Furthermore, the PDE is contractive in Wasserstein distance, which can be shown using the following coupling argument. We will call two processes coupled if both solve (3.1) with the same Brownian motion. Let X_t, \tilde{X}_t be coupled with $X_0 \sim \mu_0$ and $\tilde{X}_0 \sim \tilde{\mu}_0$. Then the distribution \mathcal{M}_t of the joint variable (X_t, \tilde{X}_t) satisfies the Fokker-Planck equation

$$\frac{\partial \mathcal{M}_t}{\partial t} = \nabla_x \cdot (\mathcal{M}_t \nabla h(x)) + \nabla_{\tilde{x}} \cdot (\mathcal{M}_t \nabla h(\tilde{x})) + (\nabla_x + \nabla_{\tilde{x}}) \cdot (\nabla_x + \nabla_{\tilde{x}}) \mathcal{M}_t. \quad (3.2)$$

Note that we can rewrite this using $(\nabla_x + \nabla_{\tilde{x}}) \cdot (\nabla_x + \nabla_{\tilde{x}}) = \Delta_{x+\tilde{x}}$ by a coordinate change $(x, \tilde{x}) \mapsto (x + \tilde{x}, x - \tilde{x})$. For any distance function of the form $d(x, \tilde{x}) = \rho(\|x - \tilde{x}\|)$, we directly see $\Delta_{x+\tilde{x}} d(x, \tilde{x}) = 0$. Using this and the property (3.2) of the joint distribution \mathcal{M}_t , a contraction in Wasserstein distance can hence be shown in the following way. We start by estimating

$$\begin{aligned} \frac{1}{2} \frac{d}{dt} \mathbb{E}_{(x,\tilde{x}) \sim \mathcal{M}_t} [\|x - \tilde{x}\|^2] &= \frac{1}{2} \frac{d}{dt} \int \|x - \tilde{x}\|^2 \mathcal{M}_t(dx, d\tilde{x}) \\ &= \frac{1}{2} \int \|x - \tilde{x}\|^2 [\nabla_x \cdot (\mathcal{M}_t \nabla h(x)) + \nabla_{\tilde{x}} \cdot (\mathcal{M}_t \nabla h(\tilde{x})) + \Delta_{x+\tilde{x}} \mathcal{M}_t] dx d\tilde{x} \\ &= - \int (x - \tilde{x}) \cdot (\nabla h(x) - \nabla h(\tilde{x})) \mathcal{M}_t(dx, d\tilde{x}) \\ &\leq -\omega_h \mathbb{E}_{(x,\tilde{x}) \sim \mathcal{M}_t} [\|x - \tilde{x}\|^2], \end{aligned}$$

where we used that due to strong convexity of h , we have $(x - \tilde{x}) \cdot (\nabla h(x) - \nabla h(\tilde{x})) \geq \omega_h \|x - \tilde{x}\|^2$. Applying now Gronwall's lemma, we obtain

$$\mathbb{E}_{(x, \tilde{x}) \sim \mathcal{M}_t} [\|x - \tilde{x}\|^2] \leq e^{-2\omega_h t} \mathbb{E}_{(x, \tilde{x}) \sim \mathcal{M}_0} [\|x - \tilde{x}\|^2].$$

The left side is bounded from below by $\mathcal{W}_2^2(\mu_t, \tilde{\mu}_t)$ by definition. By taking the infimum over all couplings \mathcal{M}_0 (with marginals μ_0 and $\tilde{\mu}_0$) on the right hand side, we obtain

$$\mathcal{W}_2(\mu_t, \tilde{\mu}_t) \leq e^{-\omega_h t} \mathcal{W}_2(\mu_0, \tilde{\mu}_0).$$

In particular, if we choose one of the processes to be initialized at the target distribution as $\tilde{\mu}_0 = \mu_*$, then the distribution of \tilde{X}_t is stationary at $\tilde{\mu}_t = \mu_*$ and by the above we obtain

$$\mathcal{W}_2(\mu_t, \mu_*) \leq e^{-\omega_h t} \mathcal{W}_2(\mu_0, \mu_*).$$

3.1.2 Contraction and Stationary Solution of the Primal-Dual Diffusion Equation

We can generalize the above argument allowing an analysis of the time-continuous limit (2.6) of the primal dual sampling scheme (2.4). For that, we consider Z_t to satisfy a general stochastic differential inclusion with non-homogeneous coefficients

$$dZ_t \in -A(Z_t) dt + B(Z_t) dW_t. \quad (3.3)$$

Here W_t is Brownian motion in \mathbb{R}^K and $B : \mathbb{R}^d \rightarrow \mathbb{R}^{d \times K}$. The drift $A : \mathbb{R}^n \rightarrow 2^{\mathbb{R}^d}$ is a set-valued monotone operator in the norm $\|\cdot\|$, meaning

$$\langle w - \tilde{w}, z - \tilde{z} \rangle \geq 0, \quad \forall w \in A(z), \tilde{w} \in A(\tilde{z}).$$

We say that A is ω -strongly monotone if the following stronger condition is satisfied:

$$\langle w - \tilde{w}, z - \tilde{z} \rangle \geq \omega \|z - \tilde{z}\|^2, \quad \forall w \in A(z), \tilde{w} \in A(\tilde{z}).$$

Proposition 3.1. *Let Z_t be a solution to (3.3) and denote by π_t the density w.r.t. the Lebesgue measure of the distribution of Z_t . Then π_t satisfies the Fokker-Planck equation*

$$\frac{\partial \pi_t}{\partial t} = \nabla_z \cdot (w \pi_t + \Sigma(z) \nabla_z \pi_t), \quad w \in A(z). \quad (3.4)$$

with $\Sigma = \frac{1}{2} B B^T \in \mathbb{R}^{n \times n}$.

Since we are repeatedly going to make use of coupling arguments, note that by applying Proposition 3.1 to a coupled diffusion

$$\begin{pmatrix} dZ_t \\ d\tilde{Z}_t \end{pmatrix} \in - \begin{pmatrix} A(Z_t) \\ A(\tilde{Z}_t) \end{pmatrix} dt + \begin{pmatrix} B \\ B \end{pmatrix} dW_t, \quad (3.5)$$

we can also obtain a Fokker-Planck equation for the joint density of the coupled processes.

Proposition 3.2. *Let Z_t, \tilde{Z}_t be two coupled processes that both solve (3.3) with the same Brownian motion, i.e. (Z_t, \tilde{Z}_t) solves (3.5). Then the joint distribution $\Pi_t(z, \tilde{z})$ of (Z_t, \tilde{Z}_t) satisfies the Fokker-Planck equation*

$$\frac{\partial \Pi_t}{\partial t} = \nabla_z \cdot (w \pi_t) + \nabla_{\tilde{z}} \cdot (\tilde{w} \Pi_t) + (\nabla_z + \nabla_{\tilde{z}}) \cdot (\Sigma(\nabla_z + \nabla_{\tilde{z}}) \Pi_t), \quad w \in A(z), \tilde{w} \in A(\tilde{z}). \quad (3.6)$$

For showing the contractivity of overdamped Langevin dynamics in Section 3.1.1, the relevant requirement was the strong convexity of h , implying that ∇h is a strongly monotone operator. The computation can be directly generalized under a strong monotonicity assumption on A .

Lemma 3.3. *Suppose A is ω -strongly monotone. Then (3.3) is contractive in the sense that, if Z_t, \tilde{Z}_t are two coupled processes that solve (3.3) with the same Brownian motion, then for $t \geq 0$ their associated distributions $\pi_t, \tilde{\pi}_t$ satisfy*

$$\mathcal{W}_2(\pi_t, \tilde{\pi}_t) \leq e^{-\omega t} \mathcal{W}_2(\pi_0, \tilde{\pi}_0).$$

Proof. By employing (3.6), we obtain with the same reasoning as before

$$\begin{aligned} \frac{1}{2} \frac{d}{dt} \mathbb{E}_{(z, \tilde{z}) \sim \Pi_t} [\|z - \tilde{z}\|^2] &= \frac{1}{2} \frac{d}{dt} \int \|z - \tilde{z}\|^2 \Pi_t(dz, d\tilde{z}) \\ &= \frac{1}{2} \int \|z - \tilde{z}\|^2 (\nabla_z \cdot (w \Pi_t) + \nabla_{\tilde{z}} \cdot (\tilde{w} \Pi_t) + (\nabla_z + \nabla_{\tilde{z}}) \cdot (\Sigma(\nabla_z + \nabla_{\tilde{z}}) \Pi_t)) dz d\tilde{z} \\ &= - \int ((z - \tilde{z}) \cdot w + (\tilde{z} - z) \cdot \tilde{w}) \Pi_t(dz, d\tilde{z}) \\ &\leq -\omega \mathbb{E}_{(z, \tilde{z}) \sim \Pi_t} [\|z - \tilde{z}\|^2] \end{aligned}$$

In the second line we used Proposition 3.2 and in the third line partial integration together with the fact that $(\nabla_z + \nabla_{\tilde{z}})(\|z - \tilde{z}\|^2) = 0$. We now apply Gronwall's Lemma and obtain

$$\mathbb{E}_{(z, \tilde{z}) \sim \Pi_t} [\|z - \tilde{z}\|^2] \leq e^{-2\omega t} \mathbb{E}_{(z, \tilde{z}) \sim \Pi_0} [\|z - \tilde{z}\|^2]$$

which implies

$$\mathcal{W}_2(\pi_t, \tilde{\pi}_t) \leq e^{-\omega t} \mathbb{E}_{(z, \tilde{z}) \sim \Pi_0} [\|z - \tilde{z}\|^2].$$

Taking the infimum over all couplings of π_0 and $\tilde{\pi}_0$ on the right hand side concludes the proof. \square

Consider now again the primal-dual type diffusion (2.6) and denote π_t for the law of Z_t . By Proposition 3.1, π_t solves the Fokker-Planck equation

$$\frac{\partial \pi_t}{\partial t} = \nabla_z \cdot (w \pi_t + \Sigma_{\text{cPD}} \nabla_z \pi_t), \quad w \in A_{\text{cPD}}(z). \quad (3.7)$$

with $\Sigma_{\text{cPD}} = \frac{1}{2} B_{\text{cPD}} B_{\text{cPD}}^T$ and $A_{\text{cPD}}, B_{\text{cPD}}$ as in (2.7).

Since the drift coefficient A_{cPD} is a monotone operator, the primal-dual type diffusion falls into the class of general diffusion equations considered in Lemma 3.3. Under strong convexity of g, f^* , the drift coefficient is strongly monotone and we obtain the following stability result.

Theorem 3.4. *Assume that g, f^* are ω_g -strongly convex and ω_{f^*} -strongly convex, respectively, with $\omega_g, \omega_{f^*} > 0$. Let Z_t, \tilde{Z}_t be two coupled processes that solve the primal-dual diffusion equation (2.5) with corresponding densities π_t and $\tilde{\pi}_t$. Then it holds*

$$\mathcal{T}_{1, \lambda^{-1}}(\pi_t, \tilde{\pi}_t) \leq e^{-\omega t} \mathcal{T}_{1, \lambda^{-1}}(\pi_0, \tilde{\pi}_0),$$

where $\omega = \min\{\omega_g, \lambda \omega_{f^*}\} > 0$. In particular, the dynamics are contractive and there exists a unique stationary distribution of the continuous time primal-dual diffusion process, denoted $\pi_{\text{cPD}}^{\text{stat}}$, which solves the primal-dual Fokker-Planck equation (3.7).

Proof. We employ Lemma 3.3, hence the only part we need to show is the strong monotonicity of the negative drift coefficient A_{cPD} defined by

$$A_{\text{cPD}} = \begin{pmatrix} \partial g & K^T \\ -\lambda K & \lambda \partial f^* \end{pmatrix}.$$

We write $z = (x, y) \in \mathcal{X} \times \mathcal{X} = \mathcal{Z}$ for the joint primal and dual variable and equip \mathcal{Z} with the weighted inner product $\langle \cdot, \cdot \rangle_{1, \lambda^{-1}}$. Let now $w \in A_{\text{cPD}}(z)$ and $\tilde{w} \in A_{\text{cPD}}(\tilde{z})$. Then there are $u \in \partial g(x)$ and $v \in \partial f^*(y)$ such that $w = (u + K^T y, \lambda(v - Kx))$. Equivalently, if $\tilde{w} \in A(\tilde{z})$ then there exist $\tilde{u} \in \partial g(\tilde{x})$ and $\tilde{v} \in \partial f^*(\tilde{y})$ with $\tilde{w} = (\tilde{u} + K^T \tilde{y}, \lambda(\tilde{v} - K\tilde{x}))$. It follows that

$$\begin{aligned} \langle w - \tilde{w}, z - \tilde{z} \rangle_{1, \lambda^{-1}} &= \langle u - \tilde{u}, x - \tilde{x} \rangle + \lambda \langle v - \tilde{v}, y - \tilde{y} \rangle_{\lambda^{-1}} \\ &\quad + \langle K^T(y - \tilde{y}), x - \tilde{x} \rangle - \lambda \langle K(x - \tilde{x}), y - \tilde{y} \rangle_{\lambda^{-1}} \\ &= \langle u - \tilde{u}, x - \tilde{x} \rangle + \langle v - \tilde{v}, y - \tilde{y} \rangle \\ &\geq \omega_g \|x - \tilde{x}\|^2 + \omega_{f^*} \|y - \tilde{y}\|^2 \\ &\geq \omega \|z - \tilde{z}\|_{1, \lambda^{-1}}^2. \end{aligned}$$

□

The stationary solution of (3.7) will be denoted by $\pi_{\text{cPD}}^{\text{stat}}$ from here. We will also frequently refer to its x -marginal as $\mu_{\text{cPD}}^{\text{stat}}$.

3.2 Non-Concentration of the Stationary Solution

Having established the existence of $\pi_{\text{cPD}}^{\text{stat}}$, we can try to relate the algorithmic, time discretized scheme to it. However, while overdamped Langevin dynamics is designed to have the target μ^* as its stationary solution, this is not the case in the primal-dual setting. In general, μ^* is not the marginal distribution of X when $(X, Y) \sim \pi_{\text{cPD}}^{\text{stat}}$, i.e. $\mu^* \neq \mu_{\text{cPD}}^{\text{stat}}$. We demonstrate this in a simple example of a Gaussian target, where we can solve the Fokker-Planck equation (3.7) in closed form.

Theorem 3.5. *Consider a one-dimensional setting with the target $\mu^*(x) \propto \exp(-h(x))$ given by*

$$f(y) := \frac{1}{2c_f} y^2, \quad g(x) := \frac{1}{2c_g} x^2, \quad h(x) := f(kx) + g(x) = \frac{k^2 c_g + c_f}{2c_f c_g} x^2, \quad x, y \in \mathbb{R},$$

where $k \neq 0$ and $c_g, c_f > 0$. It holds $f^*(y) = \frac{c_f}{2} y^2$ for all $y \in \mathbb{R}$. The primal-dual flow (2.6) of the joint variable $Z_t = (X_t, Y_t)^T \in \mathbb{R}^2$ reads

$$dZ_t = -A_{\text{cPD}} Z_t dt + B_{\text{cPD}} dW_t, \quad \text{with } A_{\text{cPD}} = \begin{pmatrix} c_g^{-1} & k \\ -\lambda k & \lambda c_f \end{pmatrix}, B_{\text{cPD}} = \begin{pmatrix} \sqrt{2} \\ 0 \end{pmatrix}$$

where W_t is one-dimensional Brownian motion and the weight $\lambda > 0$ relates primal and dual time scales. Denoting $E(t) := (e_{ij}(t))_{i,j} := \exp(-tA_{\text{cPD}}^T)$, the following statements hold:

- (i) For any (possibly singular) initialization π_0 such that $Z_0 \sim \pi_0$, the distribution $\pi_t := \text{Law}(Z_t)$ has a C^∞ -smooth Lebesgue density for $t > 0$.
- (ii) If π_0 is Gaussian (including degenerate Gaussians with singular covariance matrix), then π_t is (non-degenerate) Gaussian for all $t > 0$. As $t \rightarrow \infty$, the solution π_t converges to the Gaussian stationary π^{stat} with mean zero and covariance matrix

$$\frac{1}{(c_f + k^2 c_g)(1 + \lambda c_f c_g)} \begin{pmatrix} c_g(c_f + k^2 c_g) + \lambda c_f^2 c_g^2 & k \lambda c_f c_g^2 \\ k \lambda c_f c_g^2 & k^2 \lambda c_g^2 \end{pmatrix}.$$

The x -marginal $\mu_{\text{cPD}}^{\text{stat}}$ is not equal to the target μ^* . However, the limiting joint distribution as $\lambda \rightarrow \infty$ is the degenerate Gaussian $(\text{id}, f'(k \cdot))_{\#} \mu^*$ whose x -marginal is the target μ^* .

Proof. From the diffusion equation, it follows that the distribution $\pi_t(z) = \pi_t(x, y)$ of Z_t satisfies the Fokker-Planck equation

$$\partial_t \pi_t = \nabla_z \cdot (\pi_t A_{\text{cPD}} z) + \Delta_x \pi_t,$$

with an initial value π_0 . The Cauchy problem can be solved in closed form, note that a similar computation has been carried out in [34]. By taking the Fourier transform in the variable z (denoted \mathcal{F}), we obtain the first order initial value problem for $p_t(\zeta) = \mathcal{F}(\pi_t)(\zeta)$ with $\zeta = (\xi, \omega)^T$:

$$\begin{cases} \partial_t p_t = -\zeta^T A_{\text{cPD}} \nabla_{\zeta} p_t - \xi^2 p_t \\ p_0(\xi, \omega) = \mathcal{F} \pi_0. \end{cases}$$

The corresponding characteristic equations are

$$\begin{aligned} \dot{\zeta}(t) &= A_{\text{cPD}}^T \zeta(t) \\ \dot{p}(t) &= -\xi^2(t) p(t), \end{aligned}$$

and they are solved by

$$\begin{aligned} \zeta(t) &= \exp(t A_{\text{cPD}}^T) \zeta_0 \\ p(t) &= p_0(\zeta_0) \exp\left(-\int_0^t \xi^2(s) ds\right) \end{aligned}$$

By eliminating the initial value $\zeta_0 = \exp(-t A_{\text{cPD}}^T) \zeta(t)$, the solution for the initial value problem is

$$p_t(\zeta) = p_0(\exp(-t A_{\text{cPD}}^T) \zeta) \exp\left(-\frac{1}{2} \int_0^t (B_{\text{cPD}}^T \exp(-s A_{\text{cPD}}^T) \zeta)^2 ds\right).$$

The quadratic form inside the integral is positive semidefinite in the variable ζ . For $t > 0$, it is also positive definite: Otherwise, there would need to be a ζ such that $B_{\text{cPD}}^T \exp(-s A_{\text{cPD}}^T) \zeta = 0$ for all $s \in [0, t]$, which implies $B_{\text{cPD}}^T (A_{\text{cPD}}^T)^k \zeta = 0$ for all $k \geq 0$. This is equivalent to $(0, 1)^T$ being an element of an invariant subspace of A_{cPD}^T , which is impossible since the eigenvectors of A_{cPD}^T are of the form

$$\left(\frac{c_g^{-1} - \lambda c_f}{2k} \pm \frac{1}{2k} \sqrt{(c_g^{-1} - \lambda c_f)^2 - 4\lambda k^2}, 1 \right)^T,$$

neither of which is a multiple of $(0, 1)^T$. From the positive definiteness of the quadratic form it follows that p_t is a Schwartz function for every $t > 0$. In particular, its inverse Fourier transform π_t is C^∞ -smooth in the variable z for $t > 0$, which proves (i).

If the initialization π_0 is Gaussian with mean $z_0 = (x_0, y_0)$ and (possibly singular) covariance Σ_0 , we can simply take the inverse Fourier transform to obtain the solution π_t . It is worth noting, however, that we do not even have to compute the full distribution π_t in order to analyze the x -marginal μ_t of π_t . Since marginalizing out the dual variable y in π_t corresponds to evaluating p_t at $\zeta = (\xi, 0)$ in Fourier space, we get, denoting by \mathcal{F}_ξ^{-1} the inverse Fourier transform in ξ and $E(t) := (e_{ij}(t))_{i,j} := \exp(-t A_{\text{cPD}}^T)$,

$$\begin{aligned} \mu_t(x) &:= \int \pi_t(x, y) dy \\ &= \mathcal{F}_\xi^{-1}(p_t(\xi, 0))(x) \\ &\propto \int \exp\left(i\xi(x - z_0 \cdot e_1(t)) - \frac{\xi^2}{2} \left(\|e_1(t)\|_{\Sigma_0}^2 + 2 \int_0^t e_{11}^2(s) ds \right)\right) d\xi \\ &= \exp\left(-\frac{1}{2}(x - z_0 \cdot e_1(t))^2 \left(\|e_1(t)\|_{\Sigma_0}^2 + 2 \int_0^t e_{11}^2(s) ds \right)^{-1}\right), \end{aligned}$$

where we abbreviated $e_1(t)$ for the first column of $E(t)$. Hence, the primal variable follows a Gaussian distribution at every time $t > 0$, with mean $z_0^T e_1(t)$ and variance $\|(e_1(t))\|_{\Sigma_0}^2 + 2 \int_0^t e_{11}^2(s) ds$. Due to the contraction result Theorem 3.4, we know that μ_t converges to the stationary distribution $\mu_{\text{cPD}}^{\text{stat}}$ as $t \rightarrow \infty$. Indeed, this holds here since $\lim_{t \rightarrow \infty} E(t) = 0$, so $\mathbb{E}_{X \sim \mu_{\text{cPD}}^{\text{stat}}}[X] = 0$. The variance of $\mu_{\text{cPD}}^{\text{stat}}$ is

$$\text{Var}_{X \sim \mu_{\text{cPD}}^{\text{stat}}}[X] = 2 \int_0^\infty e_{11}^2(s) ds = \frac{c_g(c_f + k^2 c_g) + \lambda c_f^2 c_g^2}{(c_f + k^2 c_g)(1 + \lambda c_f c_g)},$$

which does not coincide with the variance of the target distribution μ^* . The target is however approximated as λ becomes large, since $\lim_{\lambda \rightarrow \infty} \text{Var}[\mu_{\text{cPD}}^{\text{stat}}] = c_g c_f / (c_f + k^2 c_g)$.

Analogously, the full solution π_t of the Fokker-Planck equation can be computed by taking the inverse Fourier transform in ζ above. We obtain that π_t is Gaussian at every time $t > 0$ with mean $E(t)^T z_0$ and positive definite covariance matrix

$$\text{Var}_{Z \sim \pi_t}[Z] = E(t)^T \Sigma_0 E(t) + 2 \begin{pmatrix} \int_0^t e_{11}^2 ds & \int_0^t e_{11} e_{12} ds \\ \int_0^t e_{11} e_{12} ds & \int_0^t e_{12}^2 ds \end{pmatrix}.$$

In the limit $t \rightarrow \infty$, we obtain the stationary distribution which has mean zero and covariance matrix

$$\text{Var}_{Z \sim \pi_{\text{cPD}}^{\text{stat}}}[Z] = \frac{1}{(c_f + k^2 c_g)(1 + \lambda c_f c_g)} \begin{pmatrix} c_g(c_f + k^2 c_g) + \lambda c_f^2 c_g^2 & k \lambda c_f c_g^2 \\ k \lambda c_f c_g^2 & k^2 \lambda c_g^2 \end{pmatrix}$$

In the limit $\lambda \rightarrow \infty$, the stationary distribution approaches a degenerate Gaussian (in the sense that the covariance matrix is singular), with mean zero and covariance matrix

$$\frac{1}{(c_f + k^2 c_g)} \begin{pmatrix} c_f c_g & k c_g \\ k c_g & k^2 c_f^{-1} c_g \end{pmatrix}.$$

This is identical to $(id, f'(k \cdot))_{\#} \mu^*$, proving (ii). \square

The negative result Theorem 3.5 naturally raises the question whether the diffusion equation can be modified such that the target becomes its stationary distribution. While we will consider the more general case of non-homogeneous, problem-dependent diffusion coefficients in Section 3.4, the (algorithmically) most straightforward approach would be to add homogeneous diffusion not only in the primal variable X_k of the algorithm, but also in the dual Y_k . Unfortunately, the next theorem shows this approach can not be successful.

Theorem 3.6. *Consider the same target μ^* as in Theorem 3.5, but a more general diffusion process*

$$dZ_t = -A_{\text{cPD}} Z_t dt + B_{\text{cPD}} dW_t, \quad \text{with } A_{\text{cPD}} = \begin{pmatrix} c_g^{-1} & k \\ -\lambda k & \lambda c_f \end{pmatrix}, B_{\text{cPD}} = \begin{pmatrix} b_{11} & b_{12} \\ b_{21} & b_{22} \end{pmatrix} \quad (3.8)$$

where W_t is Brownian motion in \mathbb{R}^2 . Then there exists no choice for the entries of $B_{\text{cPD}} \in \mathbb{R}^{2 \times 2}$ independent of the constants c_g, c_f and k such that the stationary solution $\pi_{\text{cPD}}^{\text{stat}}$ of (3.8) has x -marginal μ^* .

Proof. We start by noting that the contraction result Theorem 3.4 can easily be generalized to the more general $\Sigma_{\text{cPD}} = \frac{1}{2} B_{\text{cPD}} B_{\text{cPD}}^T$ with any constant coefficient B_{cPD} , since the relevant Lemma 3.3 holds for any constant diffusion coefficient. In view of this contraction property, we can assume the initialization $Z_0 \sim \pi_0$ to be Gaussian with mean z_0 , covariance Σ_0 and obtain $\pi_{\text{cPD}}^{\text{stat}}$ by computing $\lim_{t \rightarrow \infty} \pi_t$. The reason for initializing at a Gaussian is that we can again obtain the closed-form solution π_t of the

Cauchy problem for the Fokker-Planck equation. We carry out the same computations as in the proof of Theorem 3.5, showing that π_t is Gaussian with mean $E(t)^T z_0$ and covariance matrix

$$E(t)^T \Sigma_0 E(t) + 2 \int_0^t E(s)^T B_{\text{cPD}} B_{\text{cPD}}^T E(s) ds.$$

The entries of E can be computed explicitly (we omit the terms here) and by integrating and taking the limit $t \rightarrow \infty$, we find that the x -marginal of the stationary distribution $\pi_{\text{cPD}}^{\text{stat}}$ has variance

$$\text{Var}[\mu_{\text{cPD}}^{\text{stat}}] = \frac{(b_{11}^2 + b_{12}^2)(\lambda c_f^2 c_g^2 + c_g(c_f + k^2 c_g)) - 2(b_{11}b_{21} + b_{12}b_{22})k c_f c_g^2 + (b_{21}^2 + b_{22}^2)\lambda^{-1} k^2 c_g^2}{2(1 + \lambda c_f c_g)(c_f + k^2 c_g)}.$$

We want to show that there is no choice of b_{ij} (independent of c_f, c_g and k) such that the target μ^* coincides with the x -marginal $\mu_{\text{cPD}}^{\text{stat}}$ of the stationary solution. The variance of both distributions is equal if and only if

$$2c_g c_f (1 + \lambda c_g c_f) = (b_{11}^2 + b_{12}^2)(\lambda c_f^2 c_g^2 + c_g(c_f + k^2 c_g)) - 2(b_{11}b_{21} + b_{12}b_{22})k c_f c_g^2 + (b_{21}^2 + b_{22}^2)\lambda^{-1} k^2 c_g^2.$$

Isolating the terms including k^2 shows that this implies

$$0 = (b_{11}^2 + b_{12}^2)c_g^2 + (b_{21}^2 + b_{22}^2)\lambda^{-1} k^2 c_g^2,$$

which is only satisfied if all b_{ij} are zero since $\lambda > 0$. Hence, a problem-independent choice for B_{cPD} that results in the target being invariant with respect to the diffusion does not exist. \square

We want to elaborate a little more on the concentration properties of the stationary solution $\pi_{\text{cPD}}^{\text{stat}}$. Theorem 3.5 showed that in the limiting case $\lambda \rightarrow \infty$, the stationary distribution does not have a Lebesgue density anymore since the mass concentrates on the optimality condition $\partial f^*(y) = Kx$. In that case, the primal marginal actually converges to the target distribution, which is intuitively clear since plugging in $Y_t \in \partial f(KX_t)$ into the equation for X_t reduces the equation to overdamped Langevin diffusion. We will now generalize these properties of the toy example in Theorem 3.5 in two ways. Specifically, we will show in Section 3.3 under which conditions the stationary solution converges in the limit $\lambda \rightarrow \infty$ to a singular push-forward of the target μ^* to the space of joint distributions in (x, y) . Also, we now show that the concentration at the optimality generally does not occur for finite λ , even though the diffusion coefficient is degenerate. In the case of smooth coefficients, the Fokker-Planck operator can be shown to be hypoelliptic, implying that any solution to the dynamics has a smooth density with respect to the Lebesgue measure for all times $t > 0$, even in the case of a concentrated initialization.

Definition 3.7. *Let \mathcal{L} be a partial differential operator with smooth coefficients. If, for every open set Ω and every distribution u on Ω , $\mathcal{L}u \in C^\infty(\Omega)$ implies $u \in C^\infty(\Omega)$, then \mathcal{L} is called hypoelliptic.*

Every elliptic operator is hypoelliptic, and equally any operator of the form $-\partial_t + \mathcal{L}$ where \mathcal{L} is the generator of a diffusion process with uniformly positive definite diffusion coefficient. A special case is overdamped Langevin diffusion with smooth drift, which naturally has a smooth transition density.

The degenerate diffusion coefficient in (2.5) results in a constant but only positive semidefinite diffusion coefficient Σ_{cPD} in the Fokker-Planck equation (3.7). In order to prove that the Fokker-Planck equation is hypoelliptic, we hence have to employ a weaker condition for hypoellipticity, usually termed ‘Hörmander’s condition’ [34]. In order to state it, we need the definition of the commutator operation and Lie algebras spanned by smooth vector fields.

Definition 3.8. *For two vector fields A, B on \mathbb{R}^n , the Lie bracket or commutator $[A, B]$ is the vector field on \mathbb{R}^n defined by*

$$[A, B](x) = DB(x)A(x) - DA(x)B(x),$$

with the derivative matrices $(DA)_{i,j}(x) = \partial_j A_i(x)$.

Lemma 3.9 ([34]). *Assume that the generator \mathcal{L} of a diffusion process with state space \mathbb{R}^n has C^∞ -smooth coefficients and can be written in the form*

$$\mathcal{L} = A_0 + \sum_{j=1}^n A_j^2$$

with first-order differential operators A_0, \dots, A_n . Interpreting the differential operators as vector fields, define a collection of vector fields \mathcal{A}_k by

$$\mathcal{A}_0 := \{A_j : j = 1, \dots, n\}, \quad \mathcal{A}_{k+1} = \mathcal{A}_k \cup \{[A, A_j] : A \in \mathcal{A}_k, j = 0, \dots, n\}.$$

If the vector spaces $\mathcal{A}_k(x) := \text{span}(\{A(x) : A \in \mathcal{A}_k\})$ satisfy $\bigcup_{k \geq 0} \mathcal{A}_k(x) = \mathbb{R}^n$ for every $x \in \mathbb{R}^n$, then \mathcal{L} is said to satisfy the parabolic Hörmander condition. In that case, $\partial_t - \mathcal{L}$ and $\partial_t - \mathcal{L}^*$ are both hypoelliptic, hence any process generated by \mathcal{L} has C^∞ -smooth transition probability. In particular, any solution to the Fokker-Planck equation $\partial_t p = \mathcal{L}^* p$ is $C^\infty((0, \infty) \times \mathbb{R}^n)$ -smooth.

We refer to Chapter 6 of the book [27] for a discussion in the context of diffusion SDEs and an application to the Langevin diffusion SDE with friction. For the diffusion equation arising in our primal-dual setting, the generator is given by

$$\mathcal{L}_{\text{cPD}} u = -A_{\text{cPD}}^T(z) \nabla_z u + \Delta_x u.$$

The following result gives a sufficient condition under which the primal-dual dynamics considered here satisfy Hörmander's condition, so that the corresponding Fokker-Planck operator is hypoelliptic.

Theorem 3.10. *Assume that $g \in C^\infty(\mathcal{X})$ and $f^* \in C^\infty(\mathcal{Y})$, so that the diffusion (2.6) has smooth coefficients. If $\dim(\mathcal{Y}) = m \leq d = \dim(\mathcal{X})$ and K has full rank m , then \mathcal{L}_{cPD} satisfies Hörmander's condition. As a consequence, the stationary solution $\pi_{\text{cPD}}^{\text{stat}}$ has a $C^\infty(\mathcal{Z})$ -smooth Lebesgue density.*

Proof. We apply Lemma 3.9. \mathcal{L}_{cPD} has the correct form with vector fields $A_j = \partial_{x_j}$, $j = 1, \dots, d$ and

$$A_0 = -A_{\text{cPD}}^T(z) \nabla_z = \sum_{j=1}^d \left(-\frac{\partial g}{\partial x_j}(x) - k_j^T y \right) \partial_{x_j} + \lambda \sum_{i=1}^m \left((k^i)^T x - \frac{\partial f^*}{\partial y_i}(y) \right) \partial_{y_i},$$

where we denoted the columns of K by k_1, \dots, k_d and the rows by k^1, \dots, k^m . Clearly, the vector fields A_1, \dots, A_d span the first d dimensions ∂_{x_j} , $j = 1, \dots, d$, i.e. $\mathcal{A}_0(z) = \mathcal{X}$ for all $z \in \mathcal{Z}$. The Lie brackets in \mathcal{A}_1 are given by

$$[A_j, A_0] = -(H_g(x))_j^T \nabla_x - \lambda k_j^T \nabla_y,$$

where H_g is the Hessian of g . Due to $\lambda > 0$ and the full rank assumption, the columns k_j of K span \mathcal{Y} and we have $\mathcal{A}_1(z) = \mathcal{Z}$ for all $z \in \mathcal{Z}$. \square

3.3 Convergence to Overdamped Langevin Diffusion

We now continue to show that in the limiting case $\lambda \rightarrow \infty$ and under some smoothness assumption on f , the stationary solution $\pi_{\text{cPD}}^{\text{stat}}$ actually becomes singular, and further that the primal marginal distribution coincides in the limit with the target. Note that the formal case $\lambda = \infty$ was the subject of a recent paper [3], where the authors showed convergence in the case of perfect concentration $y \in \partial f(Kx)$.

Consider the rescaled model ($\lambda = \frac{1}{\varepsilon}$) taking the form

$$\begin{cases} dX_t \in -(\partial g(X_t) + K^* Y_t) dt + \sqrt{2} dW_t \\ \varepsilon dY_t \in -(\partial f^*(Y_t) - K X_t) dt, \end{cases} \quad (3.9)$$

where we again denote the distribution of (X_t, Y_t) by π_t , with x -marginal μ_t . We are now interested in the behaviour of μ_t in the limit $\varepsilon \rightarrow 0$. Intuitively, as ε becomes small, in this formulation it becomes clear that Y_t is forced to concentrate according to the optimality condition $Y_t \in \partial f(KX_t)$. In this concentrated case, plugging in the dual variable into the primal inclusion shows that the dynamics actually coincide with overdamped Langevin dynamics, which has the correct invariant distribution. Time-discretizations of the limiting case $\varepsilon = 0$ have been considered in [3], where an intermediate iterate $Y_t \in \partial f(KX_t)$ is computed explicitly. Indeed, we can use a coupling argument between (3.9) and overdamped Langevin dynamics to bound the Wasserstein distance between the stationary state of (3.9) and the target.

Theorem 3.11. *Assume that $f \in C^3$, that g, f^* are ω_g - respectively ω_{f^*} -strongly convex, respectively, and that the target distribution μ^* satisfies*

$$\begin{aligned} \mathbb{E}_{X \sim \mu^*} [\|\nabla(\nabla f \circ K)(X)\|_F^2] &=: C_1 < \infty, \\ \mathbb{E}_{X \sim \mu^*} [\|\nabla \cdot \nabla(\nabla f \circ K)(X)\|^2] &=: C_2 < \infty, \\ \mathbb{E}_{X \sim \mu^*} [\|\nabla(\nabla f \circ K)(X) (\nabla g(X) + K^T \nabla f(KX))\|^2] &=: C_3 < \infty, \end{aligned}$$

where in the second line the Laplacian is understood acting component-wise on the \mathcal{Y} -valued function $\nabla f \circ K$. For $0 < \varepsilon < \omega_{f^*}/\omega_g$ and a constant $C(\varepsilon) = \sqrt{\varepsilon C_1}/\omega_g + \mathcal{O}(\varepsilon^{3/2})$, the following two statements hold:

1. If the primal-dual dynamics (3.9) are initialized with $X_0 \sim \mu_0$ and Y_0 concentrated at the optimality condition $Y_0 = \nabla f(KX_0)$, then for every $t > 0$ it holds

$$\mathcal{W}_2(\mu_t, \mu^*) \leq \left((1 + \varepsilon \omega_{f^*} \|K\|)^{1/2} \mathcal{W}_2(\mu_0, \mu^*) + C(\varepsilon) \right) e^{-\omega_g t} + C(\varepsilon).$$

2. The x -marginal $\mu_{\text{cPD}}^{\text{stat}}$ of the stationary solution $\pi_{\text{cPD}}^{\text{stat}}$ of (3.9) satisfies

$$\mathcal{W}_2(\mu_{\text{cPD}}^{\text{stat}}, \mu^*) \leq C(\varepsilon).$$

Proof. Assume (X_t, Y_t) with distribution π_t solves (3.9). We construct a coupling with a process \tilde{X}_t which is initialized as $\tilde{X}_0 \sim \mu^*$ and solves the usual overdamped Langevin dynamics

$$d\tilde{X}_t \in -(\partial g(\tilde{X}_t) + K^T \nabla f(K\tilde{X}_t)) dt + \sqrt{2} dW_t \quad (3.10)$$

with the same Brownian motion W_t as in (3.9). Since μ^* is the invariant distribution of (3.10), it follows $\tilde{X}_t \sim \mu^*$ for all $t > 0$. The joint measure Π_t of (X_t, Y_t, \tilde{X}_t) solves the Fokker-Planck equation

$$\begin{aligned} \frac{\partial}{\partial t} \Pi_t &= \nabla_x \cdot ((p + K^* y) \Pi_t) + \frac{1}{\varepsilon} \nabla_y \cdot ((q - Kx) \Pi_t) + \nabla_{\tilde{x}} \cdot ((\tilde{p} + K^T \tilde{y}) \Pi_t) \\ &+ (\nabla_x + \nabla_{\tilde{x}}) \cdot (\nabla_x + \nabla_{\tilde{x}}) \Pi_t. \end{aligned} \quad (3.11)$$

where as before $p \in \partial g(x), q \in \partial f^*(y), \tilde{p} \in \partial g(\tilde{x})$. With the artificial, concentrated dual variable $\tilde{Y}_t = \nabla f(\tilde{X}_t)$, we denote the singular joint law of $(\tilde{X}_t, \tilde{Y}_t)$ by $\pi^* = (I, \nabla f \circ K)_{\#} \mu^*$.

We now consider the transport distance $\mathcal{T}_{1,\varepsilon}$ on $\mathcal{P}(\mathcal{Z})$ in order to bound the distance between π_t and π^* , which due to the concentration of π^* can be written as

$$\mathcal{T}_{1,\varepsilon}(\pi_t, \pi^*) = \inf_{\Pi \in \Gamma(\pi_t, \pi^*)} \left(\mathbb{E}_{(x,y,\tilde{x}) \sim \Pi} [d_{1,\varepsilon}(x, y, \tilde{x})^2] \right)^{1/2},$$

with an augmented distance function

$$d_{1,\varepsilon}(x, y, \tilde{x}) := (\|x - \tilde{x}\|^2 + \varepsilon\|y - \nabla f(K\tilde{x})\|^2)^{1/2}.$$

By using the joint Fokker-Planck equation (3.11) and the notations $\tilde{y}(\tilde{x}) := \nabla f(K\tilde{x})$ as well as $M := \nabla \tilde{y}$ and $m := \nabla \cdot \nabla \tilde{y}$, we obtain

$$\begin{aligned} & \frac{1}{2} \frac{d}{dt} \mathbb{E}_{(x,y,\tilde{x}) \sim \Pi_t} [d_{1,\varepsilon}(x, y, \tilde{x})^2] \\ &= \frac{1}{2} \int d_{1,\varepsilon}(x, y, \tilde{x})^2 \left(\nabla_x \cdot ((p + K^T y) \Pi_t) + \frac{1}{\varepsilon} \nabla_y \cdot ((q - Kx) \Pi_t) + \nabla_{\tilde{x}} \cdot ((\tilde{p} + K^T \tilde{y}(\tilde{x})) \Pi_t) \right) d(x, y, \tilde{x}) \\ & \quad + \frac{1}{2} \int d_{1,\varepsilon}(x, y, \tilde{x})^2 ((\nabla_x + \nabla_{\tilde{x}}) \cdot (\nabla_x + \nabla_{\tilde{x}}) \Pi_t) d(x, y, \tilde{x}) \\ &= - \int ((x - \tilde{x}) \cdot (p + K^T y) + (y - \tilde{y}(\tilde{x})) \cdot (q - Kx) + (\tilde{x} - x) \cdot (\tilde{p} + K^T \tilde{y}(\tilde{x}))) d\Pi_t \\ & \quad - \varepsilon \int (M(\tilde{x})(\tilde{y}(\tilde{x}) - y)) \cdot (\tilde{p} + K^T \tilde{y}(\tilde{x})) d\Pi_t - \varepsilon \int (M(\tilde{x})(\tilde{y}(\tilde{x}) - y)) \cdot (\nabla_x + \nabla_{\tilde{x}}) \Pi_t d(x, y, \tilde{x}) \\ &= - \int (x - \tilde{x}) \cdot (p - \tilde{p}) d\Pi_t - \int (y - \tilde{y}(\tilde{x})) \cdot (q - K\tilde{x}) d\Pi_t \\ & \quad + \varepsilon \int [(\tilde{y}(\tilde{x}) - y) \cdot (m(\tilde{x}) - M^T(\tilde{x})(\tilde{p} + K^T \tilde{y}(\tilde{x}))) + \|M(\tilde{x})\|_F^2] d\Pi_t \end{aligned}$$

For the terms in the second to last line, we can use strong convexity of g and f^* to estimate

$$\begin{aligned} & \int (x - \tilde{x}) \cdot (p - \tilde{p}) d\Pi_t \geq \omega_g \mathbb{E}_{(x,y,\tilde{x}) \sim \Pi_t} [\|x - \tilde{x}\|^2] \\ & \int (y - \tilde{y}(\tilde{x})) \cdot (q - K\tilde{x}) d\Pi_t \geq \frac{\omega_{f^*}}{\varepsilon} \mathbb{E}_{(x,y,\tilde{x}) \sim \Pi_t} [\|y - \tilde{y}(\tilde{x})\|_\varepsilon^2] \end{aligned}$$

Since the \tilde{x} -marginal of Π_t is the target μ^* , by assumption we have

$$\varepsilon \int \|M(\tilde{x})\|_F^2 d\Pi_t \leq \varepsilon C_1.$$

In a similar way, using the Cauchy-Schwarz inequality and Young's inequality, for any $\delta > 0$ we can bound the final term by

$$\begin{aligned} & \varepsilon \int (\tilde{y}(\tilde{x}) - y) \cdot (m(\tilde{x}) - M^T(\tilde{x})(\tilde{p} + K^T \tilde{y}(\tilde{x}))) d\Pi_t \\ & \leq \varepsilon \int \|\tilde{y}(\tilde{x}) - y\| \cdot \|m(\tilde{x}) - M^T(\tilde{x})(\tilde{p} + K^T \tilde{y}(\tilde{x}))\| d\Pi_t \\ & \leq \frac{\delta}{2} \mathbb{E}_{(x,y,\tilde{x}) \sim \Pi_t} [\|y - \tilde{y}(\tilde{x})\|_\varepsilon^2] + \frac{\varepsilon}{2\delta} \mathbb{E}_{\tilde{x} \sim \mu^*} [\|m(\tilde{x}) - M^T(\tilde{x})(\tilde{p} + K^T \tilde{y}(\tilde{x}))\|^2] \\ & \leq \frac{\delta}{2} \mathbb{E}_{(x,y,\tilde{x}) \sim \Pi_t} [\|y - \tilde{y}(\tilde{x})\|_\varepsilon^2] + \frac{\varepsilon(C_2 + C_3)}{2\delta}. \end{aligned}$$

Denoting $\varphi(t) := \mathbb{E}_{(x,y,\tilde{x}) \sim \Pi_t} [d_{1,\varepsilon}(x, y, \tilde{x})^2]$, we therefore have

$$\varphi'(t) \leq -2\omega\varphi(t) + 2\varepsilon C_1 + \frac{\varepsilon(C_2 + C_3)}{\delta},$$

where we abbreviate $\omega := \min\{\omega_g, \frac{\omega_{f^*}}{\varepsilon} - \frac{\delta}{2}\}$. Using Gronwall's lemma, this implies

$$\begin{aligned} \varphi(t) & \leq e^{-2\omega t} \varphi(0) + \int_0^t e^{-2\omega(t-s)} \left(2\varepsilon C_1 + \frac{\varepsilon(C_2 + C_3)}{\delta} \right) ds \\ & = e^{-2\omega t} \varphi(0) + \left(2\varepsilon C_1 + \frac{\varepsilon(C_2 + C_3)}{\delta} \right) \frac{1 - e^{-2\omega t}}{2\omega} \end{aligned}$$

By the definition of $\mathcal{T}_{1,\varepsilon}$ and taking the infimum over all possible initializations Π_0 with (x, y) -marginal π_0 and (\tilde{x}, \tilde{y}) -marginal $\pi^* = (id, \nabla f \circ K)_{\#}\mu^*$ on the right side, we get

$$\mathcal{T}_{1,\varepsilon}^2(\pi_t, \pi^*) \leq \varphi(t) \leq e^{-2\omega t} \mathcal{T}_{1,\varepsilon}^2(\pi_0, \pi^*) + \left(2\varepsilon C_1 + \frac{\varepsilon(C_2 + C_3)}{\delta} \right) \frac{1 - e^{-2\omega t}}{2\omega}. \quad (3.12)$$

For $\varepsilon < \omega_{f^*}/\omega_g$, the bound on the right is minimized by $\delta = 2(\frac{\omega_{f^*}}{\varepsilon} - \omega_g)$ for any finite t as well as in the limit $t \rightarrow \infty$. This choice implies $\omega = \omega_g$ and we denote the resulting constant terms by

$$C(\varepsilon) := \left(\frac{\varepsilon C_1}{\omega_g} + \frac{\varepsilon(C_2 + C_3)}{4\omega_g(\omega_{f^*} - \varepsilon\omega_g)} \right)^{1/2} = \sqrt{\varepsilon C_1/\omega_g} + \mathcal{O}(\varepsilon^{3/2}).$$

The first desired inequality for $t > 0$ follows by taking the square root of (3.12) and using that $\mathcal{W}_2(\mu_t, \mu^*) \leq \mathcal{T}_{1,\varepsilon}(\pi_t, \pi^*)$ and, assuming a concentrated initialization $Y_0 = \nabla f(KX_0)$, that

$$\mathcal{T}_{1,\varepsilon}(\pi_0, \pi^*) \leq (1 + \varepsilon\omega_{f^*}\|K\|)^{1/2} \mathcal{W}_2(\mu_0, \mu^*).$$

Since π_t converges to the stationary distribution of interest $\pi_{\text{cPD}}^{\text{stat}}$, taking the limit $t \rightarrow \infty$ in (3.12) and using $\mathcal{W}_2(\mu_{\text{cPD}}^{\text{stat}}, \mu^*) \leq \mathcal{T}_{1,\varepsilon}(\pi_{\text{cPD}}^{\text{stat}}, \pi^*)$ proves the second statement. \square

3.4 A Bias-Corrected Modification of Primal-Dual Diffusion

In this section, we want to follow up on the negative result of Theorem 3.6, where we saw that there is no way to construct a diffusion SDE with the primal-dual type drift coefficient and homogeneous diffusion that has the correct stationary distribution. Naturally, we can also consider modifications of the diffusion SDE with problem-dependent and/or non-homogeneous diffusion coefficient, so that the samples become (in continuous time) unbiased.

We aim to correct the Fokker-Planck equation (3.7) by adding terms such that $\pi^* = (I, \nabla f \circ K)_{\#}\mu^*$ becomes the stationary solution of the PDE. Throughout this subsection, we will assume that $g \in C^1(\mathbb{R}^d)$ and $f \in C^3(\mathbb{R}^m)$, we will denote as before $M : \mathbb{R}^d \rightarrow \mathbb{R}^{d \times m}$ for $M(x) := \nabla(\nabla f \circ K)^T(x) = K^T H_f(Kx)$. Instead of (2.5), consider the modified stochastic differential equation

$$dZ_t = -A_{\text{mod}}(Z_t) dt + B_{\text{mod}}(Z_t) dW_t, \quad (3.13)$$

where the drift and diffusion coefficients are given by

$$\begin{aligned} A_{\text{mod}}(z) &:= \left(\begin{array}{c} \nabla g(x) + K^T y \\ \lambda(\nabla f^*(y) - Kx) + M(x)^T(\nabla g(x) + K^T \nabla f(Kx)) \end{array} \right) \\ B_{\text{mod}}(z) &:= \sqrt{2} \nabla(id, \nabla f \circ K)(x) = \sqrt{2} \begin{pmatrix} I \\ M(x)^T \end{pmatrix}. \end{aligned}$$

Note that B_{mod} differs from B_{cPD} in a non-homogeneous coefficient in the dual part y . The drift A_{mod} contains the same terms as A_{cPD} , and an additional term $-M(x)^T \nabla \log \mu^*(x)$.

Remark 3.12. *As an intuitive explanation why (3.13) has the desired stationary distribution, note that we want the stationary solution to concentrate its mass in $\mathcal{Z} = \mathbb{R}^{d+m}$ on the d -dimensional manifold \mathcal{U} described by $y = \nabla f(Kx)$. The tangent space to \mathcal{U} at any point $(x, \nabla f(Kx))$, denoted in the following by $\mathcal{T}_x \mathcal{U}$, is spanned by the columns of $\nabla(id, \nabla f \circ K) = (I, M(x))^T$. This coincides with the column space of the modified diffusion coefficient $\Sigma_{\text{mod}} := \frac{1}{2} B_{\text{mod}} B_{\text{mod}}^T$, hence locally on \mathcal{U} , the diffusion is confined to the manifold. The term $\nabla f^*(y) - Kx$ in the drift vanishes upon concentration of the mass on \mathcal{U} , the remaining terms are just the gradient of the negative log-density $-\nabla \log \mu^*(x) = \nabla g(x) + K^T \nabla f(Kx)$ in the primal variable x mapped to the tangent space of \mathcal{U} by the map $(I, M(x))^T$. The drift hence does not transport mass away from \mathcal{U} and locally on \mathcal{U} , (3.13) coincides with overdamped Langevin diffusion.*

In order to show formally that the partially singular distribution π^* is a stationary solution of (3.13), we have to consider the weak formulation of the corresponding Fokker-Planck equation, given by

$$\frac{d}{dt} \int \varphi d\pi_t = \int \nabla_z^T \Sigma_{\text{mod}}(z) \nabla_z \varphi d\pi_t - \int \nabla \varphi \cdot A_{\text{mod}}(z) d\pi_t \quad \forall \varphi \in C^\infty(\mathcal{Z}). \quad (3.14)$$

Theorem 3.13. *The distribution $\pi^* := (I, \nabla f \circ K)_{\#} \mu^*$ is a stationary solution of (3.14).*

In principle, this theorem might suggest that a time discretization of the modified (3.13) may be a better idea than the primal-dual sampling algorithm (2.4). Note, however, apart from the higher-order derivative terms in f (which counter the motivation to use a primal-dual scheme in the first place), the term A_{mod} contains just the gradient of the target log-density, i.e. we explicitly add overdamped Langevin diffusion in the dual variable. This suggests that algorithmically, the dualization is somewhat redundant and any sampler would be inferior to a standard unadjusted Langevin algorithm. In order to prove Theorem 3.13, we need the following vector calculus identity.

Lemma 3.14. *Let $\psi : \mathbb{R}^d \times \mathbb{R}^m \rightarrow \mathbb{R}^n$, $\eta : \mathbb{R}^d \rightarrow \mathbb{R}^m$ and $S : \mathbb{R}^d \rightarrow \mathbb{R}^{d \times n}$, each with C^1 entries. Define $r : \mathbb{R}^d \rightarrow \mathbb{R}^n$ by $r_j(x) := \sum_i \frac{\partial S_{ij}}{\partial x_i}(x)$ and denote the partial Jacobians of ψ by $D_x \psi : \mathbb{R}^d \times \mathbb{R}^m \rightarrow \mathbb{R}^{n \times d}$ with $(D_x \psi)_{i,j}(x, y) := \frac{\partial \psi_i}{\partial x_j}(x, y)$ and $D_y \psi : \mathbb{R}^d \times \mathbb{R}^m \rightarrow \mathbb{R}^{n \times m}$ where $(D_y \psi)_{i,k}(x, y) := \frac{\partial \psi_i}{\partial y_k}(x, y)$. Then for all $x \in \mathbb{R}^d$ it holds*

$$\nabla_x \cdot (S(x) \psi(x, \eta(x))) = r(x) \cdot \psi(x, \eta(x)) + \text{tr}(S(x) D_x \psi(x, \eta(x))) + \text{tr}(S(x) D_y \psi(x, \eta(x)) D_x \eta(x)). \quad (3.15)$$

Proof. The proof is a straightforward application of product and chain rule.

$$\begin{aligned} & \nabla_x \cdot (S(x) \psi(x, \eta(x))) \\ &= \sum_{i=1}^d \frac{\partial}{\partial x_i} \left(\sum_{j=1}^d S_{ij}(x) \psi_j(x, \eta(x)) \right) \\ &= \sum_{ij} \frac{\partial S_{ij}}{\partial x_i}(x) \psi_j(x, \eta(x)) + S_{ij}(x) \frac{\partial \psi_j}{\partial x_i}(x, \eta(x)) + S_{ij}(x) \sum_{k=1}^m \frac{\partial \psi_j}{\partial y_k}(x, \eta(x)) \frac{\partial \eta_k}{\partial x_i}(x) \\ &= r(x) \cdot \psi(x, \eta(x)) + \text{tr}(S(x) D_x \psi(x, \eta(x))) + \text{tr}(S(x) D_y \psi(x, \eta(x)) D_x \eta(x)). \end{aligned}$$

□

Proof of Theorem 3.13. It suffices to check that the right side of (3.14) evaluates to zero for any $\varphi \in C^\infty(\mathbb{R}^d \times \mathbb{R}^d)$ when we insert π^* :

$$\int \begin{pmatrix} \nabla_x \\ \nabla_y \end{pmatrix}^T \begin{pmatrix} I & M(x) \\ M(x)^T & M(x)M(x)^T \end{pmatrix} \begin{pmatrix} \nabla_x \\ \nabla_y \end{pmatrix} \varphi d\pi^* - \int \nabla_x \varphi \cdot (\nabla g(x) + K^* y) d\pi^* \quad (3.16a)$$

$$- \int \nabla_y \varphi \cdot (\lambda \nabla f^*(y) - \lambda Kx) d\pi^* - \int \nabla_y \varphi \cdot M(x)^T (\nabla g(x) + K^T \nabla f(Kx)) d\pi^* \quad (3.16b)$$

Using $(\nabla f)^{-1} = \nabla f^*$ and the fact that π^* is partially concentrated on $y = \nabla f(Kx)$, it follows that

$$\int \nabla_y \varphi \cdot (\lambda \nabla f^*(y) - \lambda Kx) d\pi^* = 0.$$

Using partial integration and Lemma 3.14 with $S \equiv I$, $\psi = \nabla_x \varphi$ and $\eta = \nabla f \circ K$, the second integral in (3.16a) can be rewritten as

$$\begin{aligned}
& - \int \nabla_x \varphi \cdot (\nabla g(x) + K^* y) \, d\pi^* \\
&= \int \nabla_x \varphi(x, \nabla f(Kx)) \cdot (-\nabla g(x) - K^* \nabla f(Kx)) \exp(-f(Kx) - g(x)) \, dx \\
&= \int \nabla_x \varphi(x, \nabla f(Kx)) \cdot \nabla_x (\exp(-f(Kx) - g(x))) \, dx \\
&= - \int \nabla_x \cdot (\nabla_x \varphi(x, \nabla f(Kx))) \, d\mu^*(x) \\
&= - \int \operatorname{tr}(D_x \nabla_x \varphi(x, \nabla f(Kx))) \, d\mu^*(x) - \int \operatorname{tr}(D_y \nabla_x \varphi(x, \nabla f(Kx)) M(x)^T) \, d\mu^*(x) \\
&= - \int \Delta_x \varphi(x, \nabla f(Kx)) \, d\mu^*(x) - \int \nabla_y \cdot (M(x)^T \nabla_x \varphi(x, \nabla f(Kx))) \, d\mu^*(x)
\end{aligned}$$

where we used that $M(x)^T = D_x \eta(x)$ for $\eta = \nabla f \circ K$. These two terms cancel with the terms from the first column of the diffusion matrix in (3.16a). The second integral in (3.16b) can also be reformulated using partial integration and then Lemma 3.14, this time with $S = M$, $\psi = \nabla_y \varphi$ and $\eta = \nabla f \circ K$. In the notation of Lemma 3.14, we get $r : \mathbb{R}^d \rightarrow \mathbb{R}^m$ with $r_j(x) := \sum_i \frac{\partial M_{ij}}{\partial x_i}(x)$ and obtain

$$\begin{aligned}
& - \int \nabla_y \varphi(x, y) \cdot M(x)^T (\nabla g(x) + K^T \nabla f(Kx)) \, d\pi^* \\
&= \int \nabla_y \varphi(x, \nabla f(Kx)) \cdot M(x)^T (-\nabla g(x) - K^T \nabla f(Kx)) \exp(-f(Kx) - g(x)) \, dx \\
&= \int \nabla_y \varphi(x, \nabla f(Kx)) \cdot M(x)^T \nabla_x (\exp(-f(Kx) - g(x))) \, dx \\
&= - \int \nabla_x \cdot (M(x) \nabla_y \varphi(x, \nabla f(Kx))) \, d\mu^*(x) \\
&= - \int r(x) \cdot \nabla_y \varphi(x, \nabla f(Kx)) \, d\mu^*(x) - \int \operatorname{tr}(M(x) D_x \nabla_y \varphi(x, \nabla f(Kx))) \, d\mu^*(x) \\
&\quad - \int \operatorname{tr}(M(x) D_y \nabla_y \varphi(x, \nabla f(Kx)) M(x)^T) \, d\mu^*(x)
\end{aligned}$$

Since $\operatorname{tr}(M D_y \nabla_y \varphi M^T) = \operatorname{tr}(M^T M D_y \nabla_y \varphi) = \nabla_y \cdot (M^T M \nabla_y \varphi)$, the term in the last line cancels with the term from the lower right entry in the diffusion matrix. By the product rule, $\nabla_x \cdot (M \nabla_y \varphi) = \operatorname{tr}(M D_x \nabla_y \varphi) + r \cdot \nabla_y \varphi$, hence the second to last line cancels with the term from the upper right entry in the diffusion matrix. It follows that (3.16) is equal to zero. \square

Remark 3.15. *In general, it is hard to generalize a contraction result like Lemma 3.3 to the case of non-homogeneous diffusion coefficients. In section 2 of [13], this question is addressed in more detail for the heat equation with non-homogeneous diffusion. The authors show that it becomes possible to prove stability in a Wasserstein distance with a modified underlying metric, where the metric depends on the diffusion coefficient via an elliptic PDE.*

Since the modified equation (3.13) is of limited numerical interest, we only sketch some main ideas and omit a detailed proof. At every point $x \in \mathcal{X}$ one can define an inner product $\langle u, v \rangle_x := u^T V^{-1}(x) v$ where $V(x) = W(x) W(x)^T$ is symmetric positive definite. The first d columns of W consist of a basis of the tangent space $\mathcal{T}_x \mathcal{U}$ of \mathcal{U} at x , and the remaining m columns span the normal space $\mathcal{N}_x \mathcal{U}$. We then need to equip \mathcal{Z} with the induced Riemannian metric

$$d_{\text{mod}}(z, \tilde{z}) = \inf_{\zeta(0)=z, \zeta(1)=\tilde{z}} \int_0^1 \left(\dot{\zeta}(t)^T W^{-1}(\zeta(t)) \dot{\zeta}(t) \right)^{1/2} dt.$$

The difficulty then usually consists in finding a more convenient form of $d_{\text{mod}}(z, \tilde{z})$, which allows to integrate the Fokker-Planck equation against $d_{\text{mod}}^2(z, \tilde{z})$ in order to show contraction. We leave this to future work.

Example 3.16. We can check that in the one-dimensional quadratic case that was considered as an illustrative counterexample in Theorems 3.5 and 3.6, the modified equation now has the desired invariant distribution π^* . Furthermore, every solution π_t of the Fokker-Planck equation converges to π^* as $t \rightarrow \infty$. This can be seen as follows: We carry out the same computations as in the proof of Theorem 3.5 to obtain the Fourier transform p_t of the solution π_t , given by

$$p_t(\zeta) = p_0(\exp(-tA_{\text{mod}}^T)\zeta) \exp\left(-\frac{1}{2} \int_0^t (B_{\text{mod}}^T \exp(-sA_{\text{mod}}^T)\zeta)^2 ds\right),$$

$$A_{\text{mod}} = \begin{pmatrix} c_g^{-1} & k \\ -\lambda k + kc_f^{-1}c_g^{-1} + k^3c_f^{-2} & \lambda c_f \end{pmatrix}, \quad B_{\text{mod}} = \begin{pmatrix} 1 \\ kc_f^{-1} \end{pmatrix},$$

This time, the quadratic form under the integral is not positive definite in ζ since B_{mod} is an eigenvector of A_{mod} with eigenvalue $v_h := c_g^{-1} + k^2c_f^{-1}$. Instead, it holds

$$\int_0^t (B_{\text{mod}}^T \exp(-sA_{\text{mod}}^T)\zeta)^2 ds = v_h^{-1} (1 - e^{-tv_h}) (B_{\text{mod}}^T \zeta)^2.$$

Taking the inverse Fourier transform shows that for every (possibly degenerate) initialization π_0 the solution π_t converges to the invariant distribution, which is degenerated Gaussian with mean zero and covariance matrix $v_h^{-1} B_{\text{mod}} B_{\text{mod}}^T$. This is precisely the target distribution π^* .

4 Stability Analysis in Discrete Time

We want to apply similar techniques as in Section 3 to the time discretized setting of the algorithm (2.4). Indeed, couplings like the ones we employed in the continuous time setting above have been used before in the stability and convergence analysis of Langevin algorithms. We begin this section by recalling such a computation in the simple case of ULA as an instructive example, and then expand to the primal-dual algorithm considered here.

Consider two Markov chains $(X_n)_n, (\tilde{X}_n)_n$ defined by initial values X_0, \tilde{X}_0 and

$$\begin{aligned} \xi^{n+1} &\sim N(0, I) \\ X^{n+1} &= X^n - \tau \nabla h(X^n) + \sqrt{2\tau} \xi^{n+1} \\ \tilde{X}^{n+1} &= \tilde{X}^n - \tau \nabla h(\tilde{X}^n) + \sqrt{2\tau} \xi^{n+1} \end{aligned}$$

Then we can compute that (see [17], Prop. 3 where this calculation has been carried out)

$$\begin{aligned} \|X^{n+1} - \tilde{X}^{n+1}\|^2 &= \|X^n - \tau \nabla h(X^n) - \tilde{X}^n + \tau \nabla h(\tilde{X}^n)\|^2 \\ &= \|X^n - \tilde{X}^n\|^2 - 2\tau D_{h, \text{sym}}(X^n, \tilde{X}^n) + \tau^2 \|\nabla h(X^n) - \nabla h(\tilde{X}^n)\|^2. \end{aligned}$$

We can use the strong convexity of h , which guarantees

$$D_{h, \text{sym}}(X^n, \tilde{X}^n) \geq \frac{\mu_h L}{\mu_h + L} \|X^n - \tilde{X}^n\|^2 + \frac{1}{\mu_h + L} \|\nabla h(X^n) - \nabla h(\tilde{X}^n)\|^2,$$

and we obtain

$$\|X^{n+1} - \tilde{X}^{n+1}\|^2 \leq \left(1 - \tau \frac{2\mu_h L}{\mu_h + L}\right) \|X^n - \tilde{X}^n\|^2 + \tau \left(\tau - \frac{2}{\mu_h + L}\right) \|\nabla h(X^n) - \nabla h(\tilde{X}^n)\|^2.$$

If the step size is chosen to be $\tau = 2/(\mu_h + L)$, we obtain the convergence rate

$$\|X^n - \tilde{X}^n\|^2 \leq \left(\frac{L - \mu_h}{L + \mu_h}\right)^{2n} \|X^0 - \tilde{X}^0\|^2.$$

Denoting the distribution of X^n by μ^n and that of \tilde{X}^n by $\tilde{\mu}^n$, we obtain by taking the infimum over all couplings of μ^0 and $\tilde{\mu}^0$ on the right side that

$$\mathcal{W}_2(\mu_n, \tilde{\mu}_n) \leq \left(\frac{L - \mu_h}{L + \mu_h}\right)^n \mathcal{W}_2(\mu_0, \tilde{\mu}_0).$$

This shows that ULA is stable and will converge to its unique stationary distribution. Similar computations can be carried out for other time-discretized schemes based on Langevin diffusion, e.g. time-implicit leading to proximal sampling schemes. Since the stationary distribution of the time-discrete scheme is not the target distribution μ^* , the missing step to showing convergence of the Markov chain is to couple a time-discrete chain and a time-continuous process and then finding an error bound. Typically, this is more challenging and the introduced bias (in Wasserstein distance) between the two settings scales as $\sqrt{\tau}$.

We now turn to the primal-dual setting of (2.4). Consider again two Markov chains with potentially different initial values $(X^0, Y^0) \sim \pi^0$ and $(\tilde{X}^0, \tilde{Y}^0) \sim \tilde{\pi}^0$, but equal stochastic input:

$$\begin{aligned} \xi^{n+1} &\sim \mathcal{N}(0, I) & \tilde{Y}^{n+1} &= \text{prox}_{\sigma f^*}(\tilde{Y}^n + \sigma K \tilde{X}_\theta^n) \\ Y^{n+1} &= \text{prox}_{\sigma f^*}(Y^n + \sigma K X_\theta^n) & \tilde{X}^{n+1} &= \text{prox}_{\tau g}(\tilde{X}^n - \tau K^T \tilde{Y}^{n+1}) + \sqrt{2\tau} \xi^{n+1} \\ X^{n+1} &= \text{prox}_{\tau g}(X^n - \tau K^T Y^{n+1}) + \sqrt{2\tau} \xi^{n+1} & \tilde{X}_\theta^{n+1} &= \tilde{X}^{n+1} + \theta(\tilde{X}^{n+1} - \tilde{X}^n) \\ X_\theta^{n+1} &= X^{n+1} + \theta(X^{n+1} - X^n) \end{aligned} \tag{4.1}$$

By convention, we set $X^{-1} = X^0$ and $\tilde{X}^{-1} = \tilde{X}^0$. In the following, we denote the distribution of (X^n, Y^n) by π^n and the X^n -marginal by μ^n . Denote further $L := \|K\|$ where $\|\cdot\|$ is the operator norm induced by the Euclidean norm on \mathcal{X} and \mathcal{Y} . We assume that also in the discrete setting, the step sizes are coupled via the relation $\lambda = \sigma/\tau$.

We start by giving a stability result for the case where neither g nor f^* are strongly convex.

Theorem 4.1. *Let (X^n, Y^n) and $(\tilde{X}^n, \tilde{Y}^n)$ be given by the coupling (4.1) with relaxation parameter $\theta = 1$ and $\tau\sigma L^2 \leq 1$. Then for the primal variable it holds*

$$\mathcal{W}_2(\mu^N, \tilde{\mu}^N) \leq \mathcal{T}_{1, \lambda^{-1}}(\pi^0, \tilde{\pi}^0),$$

where $\mathcal{T}_{1, \lambda^{-1}}$ is the transport distance over the joint primal-dual variable defined in Section 2.3. If $\tau\sigma L^2 < 1$, then the joint variable obeys

$$\mathcal{T}_{1, \lambda^{-1}}(\pi^N, \tilde{\pi}^N) \leq C \mathcal{T}_{1, \lambda^{-1}}(\pi^0, \tilde{\pi}^0),$$

with the constant $C = (1 - \tau\sigma L^2)^{-1/2}$.

In the case of strongly convex g and f^* , we can prove the following contraction result.

Theorem 4.2. *Assume that g and f^* are ω_g - and ω_{f^*} -strongly convex respectively. Let (X^n, Y^n) and $(\tilde{X}^n, \tilde{Y}^n)$ be given by the coupling (4.1) with extrapolation parameter θ satisfying*

$$\max\{(1 + 2\omega_g \tau)^{-1}, (1 + 2\omega_{f^*} \sigma)^{-1}\} \leq \theta < 1,$$

and further $\theta\sigma\tau L^2 \leq 1$. Then with the constant $\tilde{\lambda} := \frac{1+2\omega_g\tau}{1+2\omega_{f^*}\sigma} \lambda$, it holds

$$\mathcal{W}_2(\mu^N, \tilde{\mu}^N) \leq \theta^{N/2} \mathcal{T}_{1, \tilde{\lambda}^{-1}}(\pi^0, \tilde{\pi}^0).$$

and if $\theta\sigma\tau L^2 < 1$, then with $\tilde{C} := (1 - \theta\tau\sigma L^2)^{-1/2}$ we have for the joint variable

$$\mathcal{T}_{1, \tilde{\lambda}^{-1}}(\pi^N, \tilde{\pi}^N) \leq \tilde{C}\theta^{N/2}\mathcal{T}_{1, \tilde{\lambda}^{-1}}(\pi^0, \tilde{\pi}^0).$$

It follows directly that in the latter case a stationary distribution π^{stat} exists and the distribution π^N of samples converges to π^{stat} as $N \rightarrow \infty$.

In order to prove Theorems 4.1 and 4.2, we need the following auxiliary inequality, which has been used several times in similar forms for primal-dual optimization algorithms and is not specific to the sampling scheme here, see e.g. [29].

Lemma 4.3. *Let (X^n, Y^n) and $(\tilde{X}^n, \tilde{Y}^n)$, $n \geq 1$ be given by the coupling (4.1) with arbitrary extrapolation parameter θ . Using the definition of the proximal mapping, we know that*

$$\begin{aligned} q^{n+1} &:= (Y^n - Y^{n+1})/\sigma + KX_\theta^n \\ p^{n+1} &:= (X^n - X^{n+1} + \sqrt{2\tau}\xi^{n+1})/\tau - K^T Y^{n+1}, \end{aligned}$$

define analogously $\tilde{p}^{n+1}, \tilde{q}^{n+1}$ for the second chain $(\tilde{X}^n, \tilde{Y}^n)$. Then it holds

$$\begin{aligned} &2\langle X^{n+1} - \tilde{X}^{n+1}, p^{n+1} - \tilde{p}^{n+1} \rangle + \|X^{n+1} - \tilde{X}^{n+1}\|_{\tau^{-1}}^2 + \|X^{n+1} - \tilde{X}^{n+1} - X^n + \tilde{X}^n\|_{\tau^{-1}}^2 \\ &\quad + 2\langle Y^{n+1} - \tilde{Y}^{n+1}, q^{n+1} - \tilde{q}^{n+1} \rangle + \|Y^{n+1} - \tilde{Y}^{n+1}\|_{\sigma^{-1}}^2 \\ &\quad + 2\langle K(X^{n+1} - \tilde{X}^{n+1} - X^n + \tilde{X}^n), Y^{n+1} - \tilde{Y}^{n+1} \rangle + (1 - \sigma\tau\theta L^2)\|Y^{n+1} - \tilde{Y}^{n+1} - Y^n + \tilde{Y}^n\|_{\sigma^{-1}}^2 \\ &\leq \|X^n - \tilde{X}^n\|_{\tau^{-1}}^2 + \theta\|X^n - \tilde{X}^n - X^{n-1} + \tilde{X}^{n-1}\|_{\tau^{-1}}^2 + \|Y^n - \tilde{Y}^n\|_{\sigma^{-1}}^2 \\ &\quad + 2\theta\langle K(X^n - \tilde{X}^n - X^{n-1} + \tilde{X}^{n-1}), Y^n - \tilde{Y}^n \rangle. \end{aligned}$$

Proof. By plugging in the representation of the subgradient p^{n+1} of g at X^{n+1} (and likewise for the second chain) given in the statement of the lemma, we can rewrite the symmetric Bregman divergence of g at $(X^{n+1}, \tilde{X}^{n+1})$ as

$$\begin{aligned} &2\langle X^{n+1} - \tilde{X}^{n+1}, p^{n+1} - \tilde{p}^{n+1} \rangle \\ &= 2\langle X^{n+1} - \tilde{X}^{n+1}, (X^n - X^{n+1})/\tau - K^T Y^{n+1} - (\tilde{X}^n - \tilde{X}^{n+1})/\tau + K^T \tilde{Y}^{n+1} \rangle \\ &= -\frac{2}{\tau}\langle X^{n+1} - \tilde{X}^{n+1}, X^{n+1} - \tilde{X}^{n+1} - X^n + \tilde{X}^n \rangle - 2\langle X^{n+1} - \tilde{X}^{n+1}, K^T(Y^{n+1} - \tilde{Y}^{n+1}) \rangle \\ &= \|X^n - \tilde{X}^n\|_{\tau^{-1}}^2 - \|X^{n+1} - \tilde{X}^{n+1}\|_{\tau^{-1}}^2 - \|X^{n+1} - \tilde{X}^{n+1} - X^n + \tilde{X}^n\|_{\tau^{-1}}^2 \\ &\quad - 2\langle K(X^{n+1} - \tilde{X}^{n+1}), Y^{n+1} - \tilde{Y}^{n+1} \rangle, \end{aligned}$$

where we used the identity $-\langle A - B, A \rangle = \frac{1}{2}\|B\|^2 - \frac{1}{2}\|A\|^2 - \frac{1}{2}\|A - B\|^2$ in the last equality. Repeating the same calculation for the subgradients q^{n+1} of f^* at Y^{n+1} , we further get

$$\begin{aligned} &2\langle Y^{n+1} - \tilde{Y}^{n+1}, q^{n+1} - \tilde{q}^{n+1} \rangle \\ &= 2\langle Y^{n+1} - \tilde{Y}^{n+1}, (Y^n - Y^{n+1})/\sigma + KX_\theta^n - (\tilde{Y}^n - \tilde{Y}^{n+1})/\sigma - K\tilde{X}_\theta^n \rangle \\ &= -\frac{2}{\sigma}\langle Y^{n+1} - \tilde{Y}^{n+1}, Y^{n+1} - \tilde{Y}^{n+1} - Y^n + \tilde{Y}^n \rangle + 2\langle Y^{n+1} - \tilde{Y}^{n+1}, K(X_\theta^n - \tilde{X}_\theta^n) \rangle \\ &= \|Y^n - \tilde{Y}^n\|_{\sigma^{-1}}^2 - \|Y^{n+1} - \tilde{Y}^{n+1}\|_{\sigma^{-1}}^2 - \|Y^{n+1} - \tilde{Y}^{n+1} - Y^n + \tilde{Y}^n\|_{\sigma^{-1}}^2 \\ &\quad + 2\langle K(X_\theta^n - \tilde{X}_\theta^n), Y^{n+1} - \tilde{Y}^{n+1} \rangle. \end{aligned}$$

In order to shorten the expressions, we introduce the shorthand notation $U^n := X^n - \tilde{X}^n$, $U_\theta^n = X_\theta^n - \tilde{X}_\theta^n$ and $V^n := Y^n - \tilde{Y}^n$. Adding up the two above equalities gives

$$\begin{aligned} 2\langle U^{n+1}, p^{n+1} - \tilde{p}^{n+1} \rangle + 2\langle V^{n+1}, q^{n+1} - \tilde{q}^{n+1} \rangle &= \|U^n\|_{\tau^{-1}}^2 - \|U^{n+1}\|_{\tau^{-1}}^2 - \|U^{n+1} - U^n\|_{\tau^{-1}}^2 \\ &\quad + \|V^n\|_{\sigma^{-1}}^2 - \|V^{n+1}\|_{\sigma^{-1}}^2 - \|V^{n+1} - V^n\|_{\sigma^{-1}}^2 \\ &\quad - 2\langle KU^{n+1}, V^{n+1} \rangle + 2\langle KU_\theta^n, V^{n+1} \rangle. \end{aligned} \quad (4.2)$$

By definition it holds $U_\theta^n = U^n + \theta(U^n - U^{n-1})$, so the two inner products in the last line can be rewritten in the following way

$$\begin{aligned}
& -2\langle KU^{n+1}, V^{n+1} \rangle + 2\langle KU_\theta^n, V^{n+1} \rangle \\
& = -2\langle K(U^{n+1} - U^n), V^{n+1} \rangle + 2\theta\langle K(U^n - U^{n-1}), V^{n+1} \rangle \\
& = -2\langle K(U^{n+1} - U^n), V^{n+1} \rangle + 2\theta\langle K(U^n - U^{n-1}), V^n \rangle + 2\theta\langle K(U^n - U^{n-1}), V^{n+1} - V^n \rangle \\
& \leq -2\langle K(U^{n+1} - U^n), V^{n+1} \rangle + 2\theta\langle K(U^n - U^{n-1}), V^n \rangle \\
& \quad + \theta\|U^n - U^{n-1}\|_{\tau^{-1}}^2 + \tau\sigma\theta L^2\|V^{n+1} - V^n\|_{\sigma^{-1}}^2.
\end{aligned}$$

The inequality follows from applying Cauchy-Schwarz and the inequality $ab \leq a^2/2c + cb^2/2$ for any $c > 0$ (Young's inequality, with $a = \|K(U^n - U^{n-1})\|$ and $b = \|V^{n+1} - V^n\|$ and $c = \tau L^2$ here) to the last inner product in the expression before. Inserting this bound into (4.2) gives precisely the statement of the Lemma. \square

Proof of Theorem 4.1. In the convex case, we start by noting that symmetric Bregman distances for convex functions are always non-negative, i.e.

$$\begin{aligned}
\langle X^{n+1} - \tilde{X}^{n+1}, p^{n+1} - \tilde{p}^{n+1} \rangle & \geq 0, \\
\langle Y^{n+1} - \tilde{Y}^{n+1}, q^{n+1} - \tilde{q}^{n+1} \rangle & \geq 0.
\end{aligned}$$

Setting $\theta = 1$, the inequality in Lemma 4.3 hence gives

$$\begin{aligned}
& \|X^{n+1} - \tilde{X}^{n+1}\|_{\tau^{-1}}^2 + \|X^{n+1} - \tilde{X}^{n+1} - X^n + \tilde{X}^n\|_{\tau^{-1}}^2 + \|Y^{n+1} - \tilde{Y}^{n+1}\|_{\sigma^{-1}}^2 \\
& \quad + 2\langle K(X^{n+1} - \tilde{X}^{n+1} - X^n + \tilde{X}^n), Y^{n+1} - \tilde{Y}^{n+1} \rangle + (1 - \sigma\tau L^2)\|Y^{n+1} - \tilde{Y}^{n+1} - Y^n + \tilde{Y}^n\|_{\sigma^{-1}}^2 \\
& \leq \|X^n - \tilde{X}^n\|_{\tau^{-1}}^2 + \|X^n - \tilde{X}^n - X^{n-1} + \tilde{X}^{n-1}\|_{\tau^{-1}}^2 + \|Y^n - \tilde{Y}^n\|_{\sigma^{-1}}^2 \\
& \quad + 2\langle K(X^n - \tilde{X}^n - X^{n-1} + \tilde{X}^{n-1}), Y^n - \tilde{Y}^n \rangle.
\end{aligned}$$

Iterating this inequality over $n = 0, \dots, N-1$ steps and using $X^{-1} = X^0$, $\tilde{X}^{-1} = X^0$ gives

$$\begin{aligned}
& \|X^N - \tilde{X}^N\|_{\tau^{-1}}^2 + \|Y^N - \tilde{Y}^N\|_{\sigma^{-1}}^2 + \|X^N - \tilde{X}^N - X^{N-1} + \tilde{X}^{N-1}\|_{\tau^{-1}}^2 \\
& \quad + 2\langle K(X^N - \tilde{X}^N - X^{N-1} + \tilde{X}^{N-1}), Y^N - \tilde{Y}^N \rangle + (1 - \tau\sigma L^2) \sum_{n=0}^{N-1} \|Y^{n+1} - \tilde{Y}^{n+1} - Y^n + \tilde{Y}^n\|_{\sigma^{-1}}^2 \\
& \leq \|X^0 - \tilde{X}^0\|_{\tau^{-1}}^2 + \|Y^0 - \tilde{Y}^0\|_{\sigma^{-1}}^2
\end{aligned}$$

Using Cauchy-Schwarz and Young's inequality on the remaining inner product and non-negativity of the sum of norms implies

$$\|X^N - \tilde{X}^N\|_{\tau^{-1}}^2 + (1 - \tau\sigma L^2)\|Y^N - \tilde{Y}^N\|_{\sigma^{-1}}^2 \leq \|X^0 - \tilde{X}^0\|_{\tau^{-1}}^2 + \|Y^0 - \tilde{Y}^0\|_{\sigma^{-1}}^2.$$

Taking expectations on both sides, by definition of the Wasserstein distance, the left side is lower bounded by $\tau^{-1}\mathcal{W}_2^2(\mu^N, \tilde{\mu}^N)$. Since the resulting inequality holds for all couplings of initializations (X^0, Y^0) and $(\tilde{X}^0, \tilde{Y}^0)$, taking the infimum over all couplings on the right side gives $\tau^{-1}\mathcal{T}_{1,\lambda^{-1}}^2(\pi^0, \tilde{\pi}^0)$, proving the first inequality. The second inequality in the statement of Theorem 4.1 results from lower bounding the left side not by the Wasserstein distance in the primal variable, but instead by $C^{-2}\tau^{-1}\mathcal{T}_{1,\lambda^{-1}}^2(\pi^N, \tilde{\pi}^N)$. \square

Proof of Theorem 4.2. We now assume strong convexity of g, f^* . In that case, the symmetric Bregman distances obey the following lower bounds

$$\begin{aligned}
\langle X^{n+1} - \tilde{X}^{n+1}, p^{n+1} - \tilde{p}^{n+1} \rangle & \geq \omega_g \|X^{n+1} - \tilde{X}^{n+1}\|^2, \\
\langle Y^{n+1} - \tilde{Y}^{n+1}, q^{n+1} - \tilde{q}^{n+1} \rangle & \geq \omega_{f^*} \|Y^{n+1} - \tilde{Y}^{n+1}\|^2.
\end{aligned}$$

The inequality in Lemma 4.3 now implies

$$\begin{aligned}
& \|X^{n+1} - \tilde{X}^{n+1}\|_{\tau^{-1}+2\omega_g}^2 + \|X^{n+1} - \tilde{X}^{n+1} - X^n + \tilde{X}^n\|_{\tau^{-1}}^2 + \|Y^{n+1} - \tilde{Y}^{n+1}\|_{\sigma^{-1}+2\omega_{f^*}}^2 \\
& + 2\langle K(X^{n+1} - \tilde{X}^{n+1} - X^n + \tilde{X}^n), Y^{n+1} - \tilde{Y}^{n+1} \rangle + (1 - \sigma\tau\theta L^2)\|Y^{n+1} - \tilde{Y}^{n+1} - Y^n + \tilde{Y}^n\|_{\sigma^{-1}}^2 \\
& \leq \|X^n - \tilde{X}^n\|_{\tau^{-1}}^2 + \theta\|X^n - \tilde{X}^n - X^{n-1} + \tilde{X}^{n-1}\|_{\tau^{-1}}^2 + \|Y^n - \tilde{Y}^n\|_{\sigma^{-1}}^2 \\
& + 2\theta\langle K(X^n - \tilde{X}^n - X^{n-1} + \tilde{X}^{n-1}), Y^n - \tilde{Y}^n \rangle.
\end{aligned}$$

Define now

$$\begin{aligned}
\Delta^n & := \|X^n - \tilde{X}^n\|_{\tau^{-1}+2\omega_g}^2 + \|X^n - \tilde{X}^n - X^{n-1} + \tilde{X}^{n-1}\|_{\tau^{-1}}^2 + \|Y^n - \tilde{Y}^n\|_{\sigma^{-1}+2\omega_{f^*}}^2 \\
& + 2\langle K(X^n - \tilde{X}^n - X^{n-1} + \tilde{X}^{n-1}), Y^n - \tilde{Y}^n \rangle.
\end{aligned}$$

Then under the assumptions on θ given in Theorem 4.2, it holds

$$\begin{aligned}
\theta\Delta^n & \geq \|X^n - \tilde{X}^n\|_{\tau^{-1}}^2 + \theta\|X^n - \tilde{X}^n - X^{n-1} + \tilde{X}^{n-1}\|_{\tau^{-1}}^2 + \|Y^n - \tilde{Y}^n\|_{\sigma^{-1}}^2 \\
& + 2\theta\langle K(X^n - \tilde{X}^n - X^{n-1} + \tilde{X}^{n-1}), Y^n - \tilde{Y}^n \rangle \\
& \geq \Delta^{n+1} + (1 - \sigma\tau\theta L^2)\|Y^{n+1} - \tilde{Y}^{n+1} - Y^n + \tilde{Y}^n\|_{\sigma^{-1}}^2 \\
& \geq \Delta^{n+1}
\end{aligned}$$

Iterating this inequality over $n = 0, \dots, N-1$ we obtain

$$\Delta^0 \geq \theta^{-N} \Delta^N.$$

We use again Cauchy-Schwarz and Young's inequality on the inner product in Δ^N as well as the initial condition $X^{-1} = X^0$, $\tilde{X}^{-1} = X^0$ and obtain

$$\begin{aligned}
& \|X^N - \tilde{X}^N\|_{\tau^{-1}+2\omega_g}^2 + (1 - \theta\tau\sigma L^2)\|Y^N - \tilde{Y}^N\|_{\sigma^{-1}+2\omega_{f^*}}^2 \\
& \leq \theta^N \left(\|X^0 - \tilde{X}^0\|_{\tau^{-1}+2\omega_g}^2 + \|Y^0 - \tilde{Y}^0\|_{\sigma^{-1}+2\omega_{f^*}}^2 \right)
\end{aligned}$$

From here, we proceed as in the proof of Theorem 4.1: Taking expectations on both sides, the left side can be bounded below by $(\tau^{-1} + 2\omega_g)W_2^2(\mu^N, \tilde{\mu}^N)$ or alternatively in the joint variable by $\tilde{C}^{-2}(\tau^{-1} + 2\omega_g)\mathcal{T}_{1, \tilde{\lambda}^{-1}}^2(\pi^N, \tilde{\pi}^N)$. The transport distance on the right is obtained by taking the infimum over all initialization couplings, completing the proof. \square

Remark 4.4. *In continuous time, our theory currently provides us with a bound between the stationary distribution and the target μ^* via Theorem 3.11. In discrete time, we obtained bounds between the stationary distribution and the samples' law. In order to make convergence statements between the samples and the target, we are currently working on a final coupling result to bridge the gap between discrete and continuous time stationary solutions. It will be reported in a future version of this manuscript.*

5 Numerical Examples

In the following, we demonstrate the behaviour and our new results on ULPDA on several numerical examples, first small-scale ones to demonstrate the convergence behaviour in detail and subsequently larger imaging inverse problems. We always simulate (2.5) in a time interval $[0, T]$ by running the discretized algorithm (2.4) with small step sizes τ, σ for T/τ steps. The step sizes are coupled via $\lambda\tau = \sigma$ and are chosen small enough so that $\tau\sigma L^2 \leq 1$, i.e. the assumptions of Theorem 4.1 are satisfied and the continuous-time dynamics are approximated well.

5.1 Revisiting the Quadratic Case

We start by illustrating the toy example of two one-dimensional quadratic potentials that was considered in Theorems 3.5 and 3.6. Recall that the target distribution has density $\exp(-h(x))/Z$ with the potential h defined as

$$h(x) = f(kx) + g(x) = \frac{k^2}{2c_f}x^2 + \frac{1}{2c_g}x^2 = \frac{c_g k^2 + c_f}{2c_f c_g}x^2,$$

hence the target distribution is Gaussian $N(0, c_f c_g (c_g k^2 + c_f)^{-1})$. For the numerical simulation, we choose $c_f = 1, c_g = 2, k = 1.5$. We simulate the primal-dual Langevin dynamics (2.5) for different values of λ by running ULPDA (2.4). We set $\theta = 1$ and set the step sizes τ and σ via the relations $\sigma/\tau = \lambda$ and $\sigma\tau k^2 = c$ where $c \leq 1$ is required for stability. We set $c = 10^{-4}$ in order to approximate closely the continuous time dynamics, resulting in step sizes $\tau = 10^{-2}\sqrt{\lambda}k$ and $\sigma = 10^{-2}\sqrt{\lambda^{-1}}k$. Figure 2 shows the joint distribution of primal and dual samples (X^n, Y^n) produced by (2.4). As λ grows, the joint distribution of primal and dual variable concentrates along the linear subspace $y = kx/c_f$ and the primal marginal distribution converges to the target.

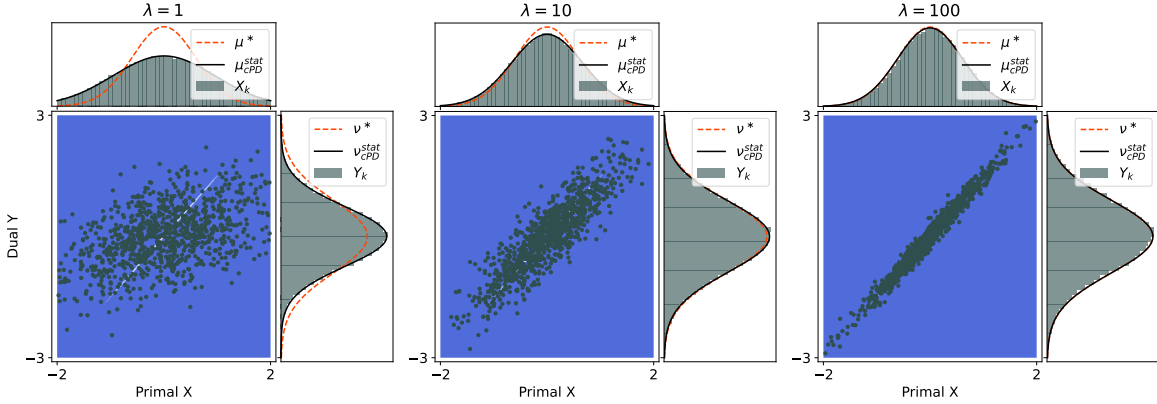


Figure 2: Approximation of the target $\mu^* = \exp(-h)$ for a one-dimensional quadratic h by (2.4) and its continuous time diffusion limit (2.5). From left to right, results for $\lambda = 1$, $\lambda = 10$ and $\lambda = 100$ are displayed. The center scatter plot shows pairs (X^n, Y^n) , the background color indicates the mass of the concentrated joint target π^* (zero is blue, the mass is concentrated along the white line $y = kx/c_f$). The marginal boxes show the densities of the primal and dual targets μ^* and $\nu^* = (\partial f \circ K)_\# \mu^*$ (dashed red), the marginals $\mu_{\text{cPD}}^{\text{stat}}, \nu_{\text{cPD}}^{\text{stat}}$ of the invariant solution of primal-dual diffusion (black solid) and samples drawn using (2.4) (grey histograms). For increasing λ , the joint distribution of samples tends to concentrate and the primal marginal converges to the target, as proven in Theorem 3.11.

5.2 TV Denoising from Gaussian Noise

For the potential $f \circ K$ being is dualized in the algorithm, we now consider the total variation (TV) functional, a typical model-based prior in imaging inverse problems. The (isotropic) TV functional is defined by

$$\text{TV}(x) := \sum_{i,j} \sqrt{(\nabla_h x)_{i,j}^2 + (\nabla_v x)_{i,j}^2},$$

where ∇_h, ∇_v denote horizontal and vertical finite differences in the pixelated image x . We consider a Gibbs prior on x with density $\exp(-\alpha \text{TV}(x))$ where α is a fixed regularization parameter (Note that

this does only defines a probability distribution on a subspace orthogonal to constant functions since TV has a one-dimensional null space. With a log-likelihood that grows fast enough at infinity along this null space, the posterior is however well-defined.). The corresponding potential term can be written in the form $\alpha \text{TV}(x) = \alpha \|Kx\|_{2,1} = f(Kx)$ where $K = (\nabla_h, \nabla_v)$ and $f = \alpha \|\cdot\|_{2,1}$ denotes a constant multiple of the nested l_2 - l_1 -norm (inner l_2 over vertical/horizontal component, outer l_1 over all pixels). We further assume that we make a noisy observation $\tilde{x} = x + \varepsilon$ of x , where the noise is distributed like $\varepsilon \sim \mathcal{N}(0, \sigma_\varepsilon^2 I)$ for some observation variance σ_ε^2 . The corresponding negative log-likelihood is

$$g(x) := l_{\tilde{x}}(x) = \frac{1}{2\sigma_\varepsilon^2} \|x - \tilde{x}\|_2^2,$$

which is σ^{-2} -strongly convex. We now want to sample from the posterior μ^* , which by Bayes law has density proportional to $\exp(-\alpha \|Kx\|_{2,1} - l_{\tilde{x}}(x)) = \exp(-f(Kx) - g(x))$.

5.2.1 Toy Example in Two Dimensions

We start with a small-scale example in which we are able to compute accurate approximations of Wasserstein distances between the samples' distribution and the true posterior. Consider the artificial case where the 'image' consists of 2×1 pixels, i.e. $\mathcal{X} = \mathbb{R}^2$. Then the operator K reduces to $Kx = x_2 - x_1 \in \mathbb{R} = \mathcal{Y}$ with $\|K\| = \sqrt{2}$, and f is given by $f(y) = \alpha |y|$. The convex conjugate f^* is the indicator function of the interval $[-\alpha, \alpha]$ and the proximal mapping $\text{prox}_{\sigma f^*}$ is, for any $\sigma > 0$, the projection onto $[-\alpha, \alpha]$.

The distribution μ^n of iterate X^n in ULPDA is approximated by running finitely many, here 10^4 , independent Markov chains in parallel and using the resulting empirical distribution $\hat{\mu}^n$. In Figure 3, we show scatter plots of the samples at time T , where T is chosen large enough that the empirical measures $\hat{\mu}^n$ remain stationary both qualitatively and in Wasserstein distance to the target (see below). As comparison, we show samples drawn using the algorithm Prox-Sub proposed in [3]. Prox-Sub solves the optimality condition $y \in \partial f(Kx)$ exactly at every step (by assuming that the subgradient can be evaluated), and hence corresponds exactly to the concentrated limit $\lambda = \infty$ of ULPDA explored in Section 3.3. The authors of [3] showed the convergence of the distribution of Prox-Sub samples to the target in 2-Wasserstein distance, total variation distance and Kullback-Leibler divergence, where the bias decreases depends as usual on the step size of the algorithm.

Using numerical integration, in this low-dimensional example we are able to compute an estimate of the normalization constant $Z = \int_{\mathcal{X}} \exp(-f(Kx) - g(x)) dx$. Using this, we can access an approximation of the posterior density $\mu^*(x)$. This allows us to compute approximations of the Wasserstein distances of current iterates to the target $\mathcal{W}_2(\hat{\mu}^n, \mu^*)$ without the need to rely on a second sampler. We evaluate the distance at 20 equidistantly spaced points in $[0, T]$ (i.e. for $\hat{\mu}^{kN}$, $k = 1, \dots, 20$ where $N = T/20\tau$). The distances are computed using the Python optimal transport module [12] and are displayed in Figure 4. As expected, the samples drawn by the Prox-Sub algorithm are closest to the target distribution (their bias in Wasserstein distance is bounded by a constant multiple of the step size τ). For finite λ , the distributions $\hat{\mu}^n$ exhibit an additional strong bias to the target due to the dualization, which becomes smaller as λ grows.

5.2.2 Image Denoising

We now sample from the posterior of an image denoising task. Due to the higher dimension, we can not compute accurate approximations of the Wasserstein distances to the target anymore. We therefore resort to illustrating the behaviour of ULPDA using moment estimates. A ground truth

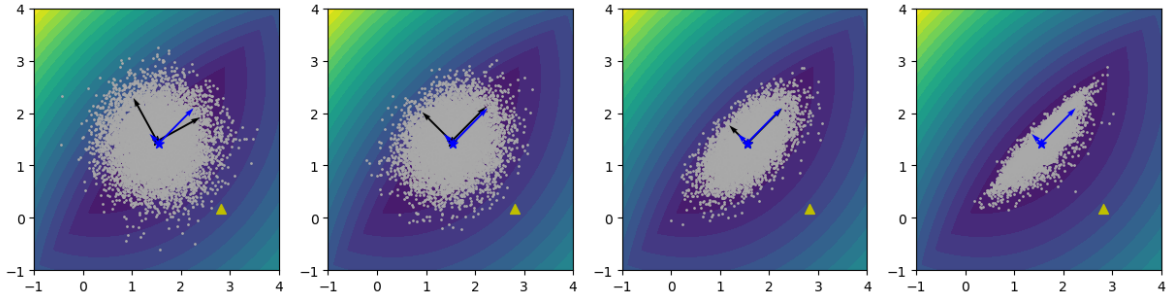


Figure 3: Scatter plots of $\hat{\mu}^n$ in the two-dimensional TV-denoising experiment. From left to right, the plots show approximations of the same posterior with values $\lambda = 10^1, 10^2, 10^3$ and ' $\lambda = \infty$ ' (Prox-Sub). Horizontal and vertical axes correspond to the two coordinates in the primal variable $x \in \mathbb{R}^2$, the dual variable y is not displayed. Grey dots show the samples at time T produced by 10^4 parallel chains, the black arrows indicate the samples' mean and the principal components of their covariance (i.e. eigenvectors of the covariance matrix scaled in length by the corresponding eigenvalues). For reference, the blue arrows are the principal components of the posterior that should be approximated. The noisy observation \tilde{x} is marked by a yellow triangle and the background color is a contour plot of the posterior density $\mu^*(x)$.

image normalized to intensities $[0, 1]$ is distorted by noise with standard deviation 0.25 (PSNR 12.02 dB in the noisy observation). We then draw 10^6 samples with a single chain and compute the sample mean and pixel-wise variance after a burn-in phase of $1e3$ samples. The experiment is repeated three times for values $\lambda = 1, 10, 100$, each with the same step size τ . A fourth chain is computed using Prox-Sub with the same τ . MMSE and pixel-wise variance estimates are reported in Figure 5. The sample mean (MMSE) estimates produced by the different chains converge quickly and are very similar for all chains (PSNR values between 23.82 dB and 23.85 dB). The pixel-wise variance, however, shows the same effect of overdispersion for smaller levels of λ as in the lower-dimensional example.

While the 'primal' samples X^n are overdispersed for finite λ , the dual iterates Y^n characteristically exhibit underdispersion (see Figure 6). This effect was consistent throughout all our numerical experiments (compare also Figures 2 and 3). A heuristic explanation for overdispersion in the primal and underdispersion in the dual variable lies in the fact that the step in the dual variable solves the optimality condition $y \in \partial f(Kx)$ only incompletely. On the particle level in continuous time, when the primal variable X_t is driven towards the tail regions of its marginal distribution by the Brownian motion, the dual variable is not evolved entirely to the corresponding position $\partial f(KX_t)$ in the tails of its marginal, but rather remains near the mode of its marginal. The effect decreased with growing parameters λ in all our experiments.

5.3 Total Generalized Variation Based Image Denoising

In this experiment, we consider an example with an image prior based on second order total generalized variation (TGV). Like the TV functional, total generalized variation allows for discontinuous edges in images, but it generalizes TV in that it also employs higher-order derivatives. This way, it avoids the typical staircasing effect of TV in smooth but non-constant regions of images. For optimization purposes, the second order TGV functional is usually defined as

$$\begin{aligned} \text{TGV}_\alpha^2(u) &= \inf_{v \in V} J_\alpha^2(u, v), \\ J_\alpha^2(u, v) &= \alpha_1 \|\nabla u - v\|_{2,1} + \alpha_0 \|Ev\|_{2,1}. \end{aligned} \tag{5.1}$$

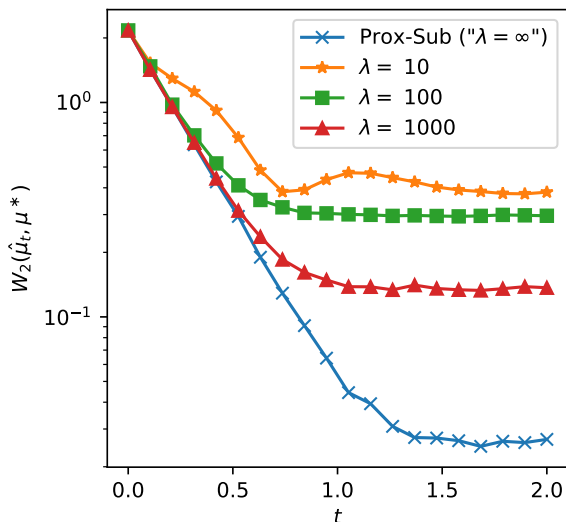


Figure 4: Wasserstein distances between the empirical measures $\hat{\mu}^n$ and the target μ^* in the two-dimensional TV-denoising experiment. We compare three different values of λ and the algorithm Prox-Sub [3] corresponding formally to $\lambda = \infty$. The discretization via partial dualization of $f \circ K$ introduces a bias between samples and target that is significantly larger than the pure discretization bias of Prox-Sub. As λ grows, the iteration approximates the purely primal setting and the bias is reduced.

Here $u \in \mathcal{U}$ is an image while v is in the corresponding space $\mathcal{V} = \mathcal{U} \times \mathcal{U}$ of (discretized) gradients of u . $\alpha_0, \alpha_1 > 0$ are regularization parameters. $\nabla = (\nabla_h, \nabla_v) : \mathcal{U} \rightarrow \mathcal{V}$ is a (forward discretized) gradient operator as in the case of TV, and $E : \mathcal{V} \rightarrow \mathcal{W}$ is a symmetrized (backward discretized) gradient operator that acts as second order derivative. We refer to Section 2.1 of [26] for details on the implementation of the gradient operators. In TGV-based variational minimization, the state space is typically expanded from the image space \mathcal{U} to the joint space $\mathcal{X} = \mathcal{U} \times \mathcal{V}$ and the minimization over u (in the variational problem) and v (in 5.1) is carried out simultaneously. By applying primal-dual optimization methods, the iteration can be carried out efficiently without the need to evaluate the infimum in (5.1) explicitly [26]. In the same way, we want to avoid evaluating TGV_α^2 or its gradients explicitly in a sampling procedure. In order to recover the image u , we therefore propose to sample from a posterior of the form

$$\mu^*(x) \propto p(\tilde{x}|x) \exp(-J_\alpha^2(u, v)), \quad x = (u, v) \in \mathcal{U} \times \mathcal{V} = \mathcal{X},$$

where $p(\tilde{x}|x)$ is the likelihood, for denoising with normally distributed noise given as before by

$$-\log p(\tilde{x}|x) = \frac{1}{2\sigma_\varepsilon^2} \|u - \tilde{u}\|_{\mathcal{U}}^2, \quad x = (u, v), \tilde{x} = (\tilde{u}, \tilde{v}) \in \mathcal{X}$$

We note that this is a relaxed version of regularization with TGV_α^2 , since we dropped the requirement that v solves (5.1). Practically, the prior $\exp(-J_\alpha^2(u, v))$ seems to yield very similar smoothing behaviour to the effect of total generalized variation, we leave its detailed analysis to future work. Note that the chosen target log-density is in the necessary form (1.1): $g(x)$ is, as before, the negative log-likelihood $\|u - \tilde{u}\|_{\mathcal{U}}^2 / (2\sigma_\varepsilon^2)$ for all $x = (u, v)$. We define the linear operator

$$K = \begin{pmatrix} \nabla & -I \\ 0 & E \end{pmatrix} : \mathcal{X} \rightarrow \mathcal{V} \times \mathcal{W} =: \mathcal{Y},$$

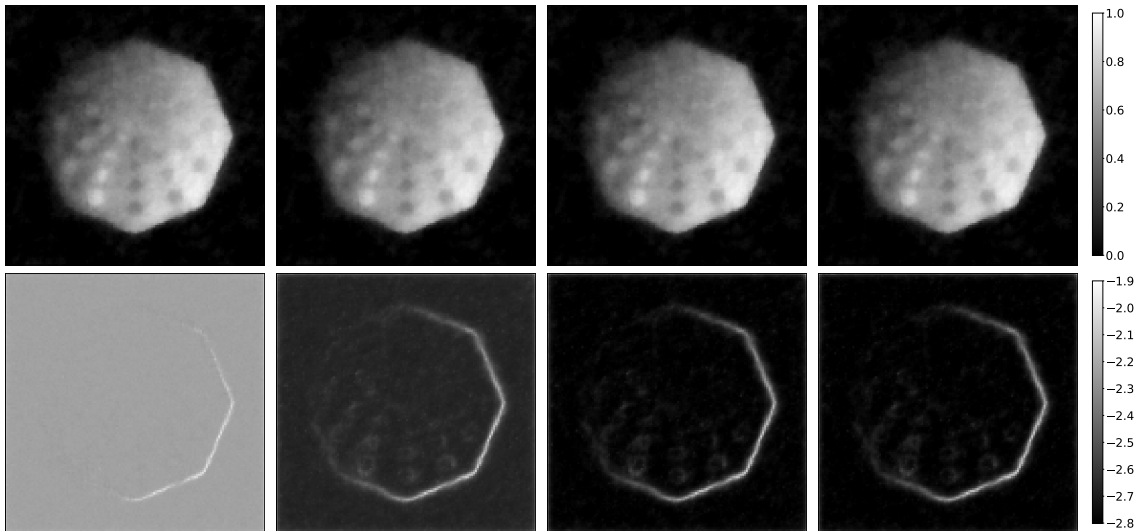


Figure 5: MMSE estimates and pixel-wise variance computed via the posterior sample mean in the l_2 -TV denoising experiment. Top row shows the MMSE estimates, bottom row the corresponding pixel-wise (logarithmically scaled) variances. From left to right results for $\lambda = 1, 10, 100$ and ' $\lambda = \infty$ ' (using Prox-Sub) are shown.

where I is the identity on \mathcal{V} . The functional $f : \mathcal{Y} \rightarrow \mathbb{R}$ is given by $f(y) = \alpha_1 \|v\|_{2,1} + \alpha_0 \|w\|_{2,1}$ for all $y = (v, w)$. Due to the separable structure in v and w , the proximal mapping of the convex conjugate f^* is simply a componentwise projection in the dual l_2 - l_∞ -norms in the respective spaces \mathcal{V}, \mathcal{W} .

We run the experiment with empirically set values of λ that make sure the variance is not strongly overdispersed while keeping the computational expense moderate – recall that as λ grows, τ needs to be chosen smaller, which slows down the convergence. 10^5 samples are drawn in each run, we report the resulting sample mean and pixel-wise variance in Figure 7.

6 Conclusion and Open Problems

We have analyzed a recently proposed algorithm for sampling from log-concave, non-smooth potentials which makes use of alternating primal-dual steps as is well-known in convex non-smooth optimization. We showed that the sampling algorithm corresponds to a stochastic differential equation and formulated the mean field limit Fokker-Planck equation. Using a simple coupling argument, contraction of the continuous-time limit to a stationary solution was proved. Unlike for purely primal overdamped Langevin diffusion, the primal-dual Fokker-Planck equation does not have the target distribution as its stationary solution. A proposed correction of the Fokker-Planck equation forcing the target to be its stationary solution is possible, but eventually not useful for numerical implementation. However, the target distribution can be related to the stationary solution of the uncorrected scheme in the limit of the ratio of primal and dual step sizes growing to infinity. We made use of coupling techniques to prove a corresponding bound in Wasserstein distance to the target for a finite step size ratio. With similar coupling arguments in discrete time, estimates in the typical spirit of convergence analysis of the optimization algorithm can be transferred to the sampling case, showing stability of the sampling method in Wasserstein distance.

We are currently working on a final coupling result, filling the gap between the stationary solution

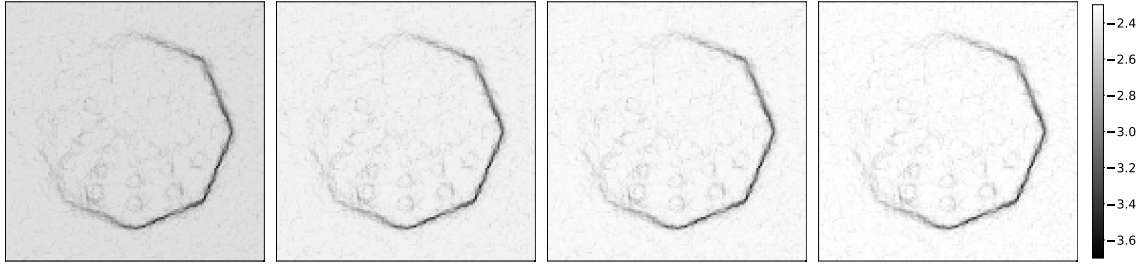


Figure 6: Pixel-wise (logarithmic) standard deviation of the dual variables Y^n , where an l_2 -norm over horizontal and vertical component was applied. From left to right, we show the results for $\lambda = 1, 10, 100$ and ‘ $\lambda = \infty$ ’ (Prox-Sub). For the latter case, the algorithm computes the dual variable as $Y^n \in \partial f(KX^n)$. For finite λ , the dual samples suffer from underdispersion, the effect vanishes as λ grows and the dual values concentrate around the dual optimality condition.

in discrete time and the stationary solution in continuous time. This, together with the stability in discrete time and the bound between continuous-time stationary state and the target would allow a convergence analysis between the algorithm and the target. Numerically, the results suggest that if there is a way to compute the subgradient of the dualized potential term, the additional bias due to the finite step size ratio makes the primal-dual samples consistently over-dispersed compared to the method of [3]. We currently see the primal-dual method’s use cases in two settings. If the subgradient of the dualized term is not available, but the proximal mapping of its convex conjugate is, the method is up to our knowledge the first applicable algorithm able to draw samples from an approximation of the posterior. Secondly, if the additional bias due to a larger finite step size ratio does not matter (because a correction step is added or because downstream tasks can be carried out with biased samples), the method can be applied with potentially larger step sizes than a purely primal method, allowing for faster mixing time. To find out whether this makes the primal-dual method more efficient in applications, further numerical studies, in particular in combination with a Metropolis-Hastings correction step, will be needed.

Acknowledgements

We thank Jan Modersitzki (Lübeck) for fruitful discussions and predicting non-concentration of the dual variable.

References

- [1] Ziruo Cai, Jinglai Li, and Xiaoqun Zhang. *Approximate Primal-Dual Fixed-Point based Langevin Algorithms for Non-smooth Convex Potentials*. 2023. DOI: 10.48550/ARXIV.2304.04544 (cit. on p. 3).
- [2] Matthias J. Ehrhardt, Lorenz Kuger, and Carola-Bibiane Schönlieb. *Proximal Langevin Sampling With Inexact Proximal Mapping*. 2023. arXiv: 2306.17737 [stat.CO] (cit. on p. 3).
- [3] Andreas Habring, Martin Holler, and Thomas Pock. *Subgradient Langevin Methods for Sampling from Non-smooth Potentials*. 2023. DOI: 10.48550/ARXIV.2308.01417 (cit. on pp. 2, 3, 14, 15, 26, 28, 30).

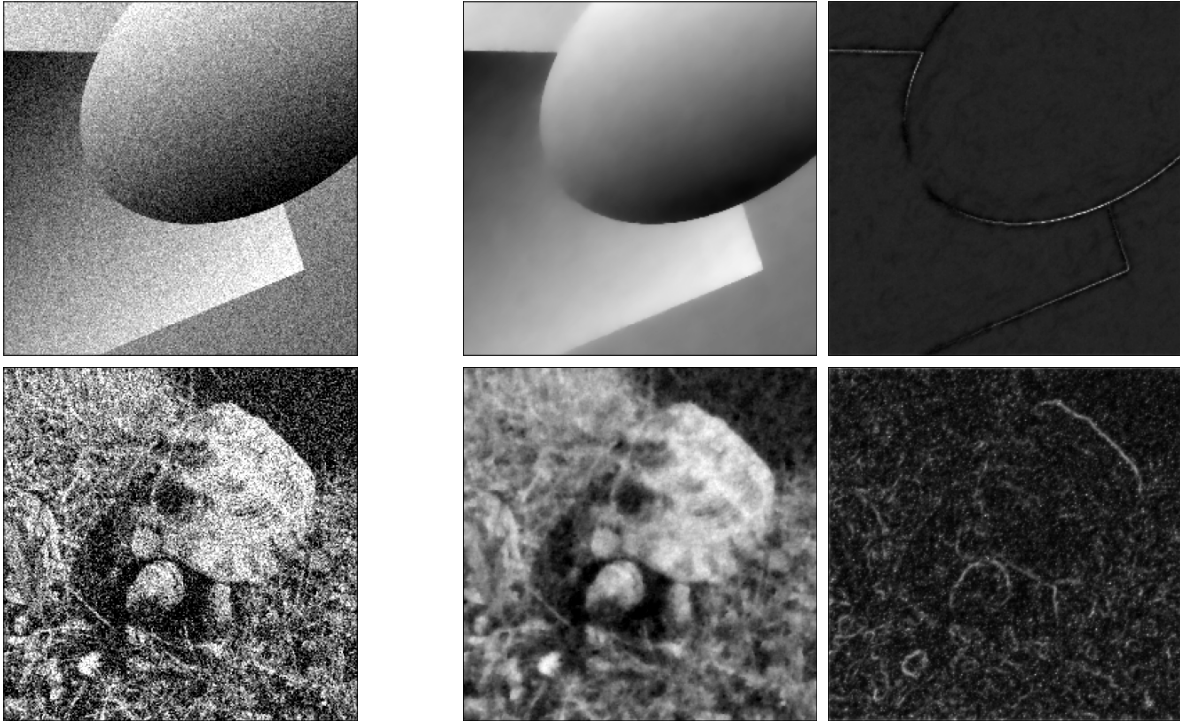


Figure 7: Results from the TGV-based denoising experiment. Left: noisy observation \tilde{u} , Center: MMSE estimate via sample mean, Right: Log-scaled pixel-wise standard deviation. Top is a moderately noisy phantom designed for TGV-regularization ($\sigma_\varepsilon = 0.1$, PSNR of noisy image 19.98 dB, MMSE PSNR 34.00 dB), bottom a more strongly distorted, photorealistic image ($\sigma_\varepsilon = 0.25$, PSNR of noisy image 12.02 dB, MMSE PSNR 20.08 dB).

- [4] Teresa Klatzer, Paul Dobson, Yoann Altmann, Marcelo Pereyra, Jesús María Sanz-Serna, and Konstantinos C. Zygalakis. *Accelerated Bayesian imaging by relaxed proximal-point Langevin sampling*. 2023. DOI: 10.48550/ARXIV.2308.09460 (cit. on p. 3).
- [5] Tim Tsz-Kit Lau, Han Liu, and Thomas Pock. *Non-Log-Concave and Nonsmooth Sampling via Langevin Monte Carlo Algorithms*. 2023. DOI: 10.48550/ARXIV.2305.15988 (cit. on pp. 2, 3).
- [6] Savvas Melidonis, Paul Dobson, Yoann Altmann, Marcelo Pereyra, and Konstantinos Zygalakis. “Efficient Bayesian Computation for Low-Photon Imaging Problems”. In: *SIAM Journal on Imaging Sciences* 16.3 (July 2023), pp. 1195–1234. ISSN: 1936-4954. DOI: 10.1137/22m1502240 (cit. on p. 3).
- [7] Alain Durmus, Éric Moulines, and Marcelo Pereyra. “A Proximal Markov Chain Monte Carlo Method for Bayesian Inference in Imaging Inverse Problems: When Langevin Meets Moreau”. In: *SIAM Review* 64.4 (Nov. 2022), pp. 991–1028. DOI: 10.1137/22m1522917 (cit. on pp. 2, 3).
- [8] Tim Tsz-Kit Lau and Han Liu. “Bregman Proximal Langevin Monte Carlo via Bregman-Moreau Envelopes”. In: *Proceedings of the 39th International Conference on Machine Learning*. Ed. by Kamalika Chaudhuri, Stefanie Jegelka, Le Song, Csaba Szepesvari, Gang Niu, and Sivan Sabato. Vol. 162. Proceedings of Machine Learning Research. PMLR, 17–23 Jul 2022, pp. 12049–12077 (cit. on p. 3).
- [9] Ruilin Li, Molei Tao, Santosh S. Vempala, and Andre Wibisono. “The Mirror Langevin Algorithm Converges with Vanishing Bias”. In: *Proceedings of The 33rd International Conference on Algo-*

- rhythmic Learning Theory*. Ed. by Sanjoy Dasgupta and Nika Haghtalab. Vol. 167. Proceedings of Machine Learning Research. PMLR, 29 Mar–01 Apr 2022, pp. 718–742 (cit. on p. 3).
- [10] Dominik Narnhofer, Andreas Habring, Martin Holler, and Thomas Pock. *Posterior-Variance-Based Error Quantification for Inverse Problems in Imaging*. 2022. DOI: 10.48550/ARXIV.2212.12499 (cit. on pp. 2, 3, 5).
- [11] Kwangjun Ahn and Sinho Chewi. “Efficient constrained sampling via the mirror-Langevin algorithm”. In: *Advances in Neural Information Processing Systems*. Ed. by A. Beygelzimer, Y. Dauphin, P. Liang, and J. Wortman Vaughan. 2021 (cit. on p. 3).
- [12] Remi Flamary et al. “POT: Python Optimal Transport”. In: *Journal of Machine Learning Research* 22.78 (2021), pp. 1–8 (cit. on p. 26).
- [13] Nicolas Fournier and Benoît Perthame. “Transport distances for PDEs: the coupling method”. In: *EMS Surveys in Mathematical Sciences* 7.1 (Jan. 2021), pp. 1–31. DOI: 10.4171/emss/35 (cit. on pp. 7, 19).
- [14] Adil Salim and Peter Richtarik. “Primal Dual Interpretation of the Proximal Stochastic Gradient Langevin Algorithm”. In: *Advances in Neural Information Processing Systems*. Ed. by H. Larochelle, M. Ranzato, R. Hadsell, M.F. Balcan, and H. Lin. Vol. 33. Curran Associates, Inc., 2020, pp. 3786–3796 (cit. on p. 3).
- [15] Arnak S. Dalalyan and Avetik Karagulyan. “User-friendly guarantees for the Langevin Monte Carlo with inaccurate gradient”. In: *Stochastic Processes and their Applications* 129.12 (Dec. 2019), pp. 5278–5311. ISSN: 0304-4149. DOI: 10.1016/j.spa.2019.02.016 (cit. on pp. 2, 5).
- [16] Alain Durmus, Szymon Majewski, and Błażej Miasojedow. “Analysis of Langevin Monte Carlo via Convex Optimization”. In: *J. Mach. Learn. Res.* 20.1 (2019), pp. 2666–2711. ISSN: 1532-4435 (cit. on p. 2).
- [17] Alain Durmus and Éric Moulines. “High-dimensional Bayesian inference via the unadjusted Langevin algorithm”. In: *Bernoulli* 25.4A (Nov. 2019), pp. 2854–2882. ISSN: 1350-7265. DOI: 10.3150/18-BEJ1073 (cit. on pp. 2, 7, 20).
- [18] Espen Bernton. “Langevin Monte Carlo and JKO splitting”. In: *Proceedings of the 31st Conference On Learning Theory*. Ed. by Sébastien Bubeck, Vianney Perchet, and Philippe Rigollet. Vol. 75. Proceedings of Machine Learning Research. PMLR, June 2018, pp. 1777–1798 (cit. on p. 3).
- [19] Sébastien Bubeck, Ronen Eldan, and Joseph Lehec. “Sampling from a Log-Concave Distribution with Projected Langevin Monte Carlo”. In: *Discrete and Computational Geometry* 59.4 (Apr. 2018), pp. 757–783. DOI: 10.1007/s00454-018-9992-1 (cit. on p. 3).
- [20] Alain Durmus, Éric Moulines, and Marcelo Pereyra. “Efficient Bayesian Computation by Proximal Markov Chain Monte Carlo: When Langevin Meets Moreau”. In: *SIAM Journal on Imaging Sciences* 11.1 (Jan. 2018), pp. 473–506. DOI: 10.1137/16M1108340 (cit. on p. 3).
- [21] Andre Wibisono. “Sampling as optimization in the space of measures: The Langevin dynamics as a composite optimization problem”. In: *Proceedings of the 31st Conference On Learning Theory*. PMLR, July 2018, pp. 2093–3027 (cit. on p. 2).
- [22] Nicolas Brosse, Alain Durmus, Éric Moulines, and Marcelo Pereyra. “Sampling from a log-concave distribution with compact support with proximal Langevin Monte Carlo”. In: *Proceedings of the 2017 Conference on Learning Theory*. Ed. by Satyen Kale and Ohad Shamir. Vol. 65. Proceedings of Machine Learning Research. PMLR, July 2017, pp. 319–342 (cit. on p. 3).
- [23] Alain Durmus and Éric Moulines. “Nonasymptotic convergence analysis for the unadjusted Langevin algorithm”. In: *The Annals of Applied Probability* 27.3 (June 2017). DOI: 10.1214/16-aap1238 (cit. on p. 2).
- [24] Antonin Chambolle and Thomas Pock. “An introduction to continuous optimization for imaging”. In: *Acta Numerica* 25 (May 2016), pp. 161–319. DOI: 10.1017/s096249291600009x (cit. on p. 5).

- [25] Marcelo Pereyra. “Proximal Markov chain Monte Carlo algorithms”. en. In: *Statistics and Computing* 26.4 (July 2016), pp. 745–760. ISSN: 1573-1375. DOI: 10.1007/s11222-015-9567-4 (cit. on p. 3).
- [26] Kristian Bredies and Martin Holler. “A TGV-Based Framework for Variational Image Decompression, Zooming, and Reconstruction. Part II: Numerics”. In: *SIAM Journal on Imaging Sciences* 8.4 (Jan. 2015), pp. 2851–2886. ISSN: 1936-4954. DOI: 10.1137/15m1023877 (cit. on p. 28).
- [27] Grigorios A. Pavliotis. *Stochastic Processes and Applications*. Springer New York, 2014. DOI: 10.1007/978-1-4939-1323-7 (cit. on pp. 7, 14).
- [28] Heinz H. Bauschke and Patrick L. Combettes. *Convex Analysis and Monotone Operator Theory in Hilbert Spaces*. Springer New York, 2011. DOI: 10.1007/978-1-4419-9467-7 (cit. on p. 5).
- [29] Antonin Chambolle and Thomas Pock. “A First-Order Primal-Dual Algorithm for Convex Problems with Applications to Imaging”. In: *Journal of Mathematical Imaging and Vision* 40.1 (May 2011), pp. 120–145. ISSN: 1573-7683 (cit. on pp. 5, 22).
- [30] Mark Girolami and Ben Calderhead. “Riemann Manifold Langevin and Hamiltonian Monte Carlo Methods”. In: *Journal of the Royal Statistical Society Series B: Statistical Methodology* 73.2 (Mar. 2011), pp. 123–214. ISSN: 1467-9868. DOI: 10.1111/j.1467-9868.2010.00765.x (cit. on p. 3).
- [31] E.J. Candes, J. Romberg, and T. Tao. “Robust uncertainty principles: exact signal reconstruction from highly incomplete frequency information”. In: *IEEE Transactions on Information Theory* 52.2 (Feb. 2006), pp. 489–509. ISSN: 0018-9448. DOI: 10.1109/tit.2005.862083 (cit. on p. 4).
- [32] Richard Jordan, David Kinderlehrer, and Felix Otto. “The Variational Formulation of the Fokker–Planck Equation”. In: *SIAM Journal on Mathematical Analysis* 29.1 (Jan. 1998), pp. 1–17. DOI: 10.1137/s0036141096303359 (cit. on p. 2).
- [33] Gareth O. Roberts and Richard L. Tweedie. “Exponential Convergence of Langevin Distributions and Their Discrete Approximations”. In: *Bernoulli* 2.4 (Dec. 1996), p. 341. DOI: 10.2307/3318418 (cit. on p. 2).
- [34] Lars Hörmander. “Hypoelliptic second order differential equations”. In: *Acta Mathematica* 119.0 (1967), pp. 147–171. DOI: 10.1007/bf02392081 (cit. on pp. 11, 13, 14).